THESIS ON NATURAL AND EXACT SCIENCES B50

Quantum-chemical modeling of solvated first row transition metal ions

MERLE UUDSEMAA

Department of Chemistry
Faculty of Science
TALLINN UNIVERSITY OF TECHNOLOGY

Dissertation was accepted for the commencement of the degree of Doctor of Philosophy in Natural and Exact Sciences on 2nd May 2006.

Supervisor: Professor Toomas Tamm, Ph.D.,
Department of Chemistry, Tallinn University of Technology,
Estonia

Opponents: Professor Peeter Burk, Ph.D.,
Institute of Chemical Physics, University of Tartu, Estonia

Research Scientist Dage Sundholm, Ph.D., Doc.,
Laboratory for Instruction in Swedish, University of Helsinki,
Finland

Commencement: June 16, 2006 at Tallinn University of Technology

Declaration: Hereby I declare that this doctoral thesis, my original investigation and achievement, submitted for the doctoral degree at Tallinn University of Technology has not been submitted for any degree or examination

Copyright Merle Uudsemaa 2006
ISSN 1406-4723
ISBN 9985-59-622-6

.

LOODUS- JA TÄPPISTEADUSED

Solvateeritud üleminekumetalli-ioonide kvantkeemiline modelleerimine

MERLE UUDSEMAA

Contents

List of publications 6

Abbreviations 7

Introduction 8

1 Review of literature 10
- 1.1 Hydration enthalpy 10
- 1.2 Redox potentials 10
  - 1.2.1 Computational electrochemistry 11

2 Aims of the study 12

3 Theoretical background 13
- 3.1 Quantum chemical methods 13
- 3.2 Solvent effects 14
- 3.3 Crystal field theory 16

4 Computational aspects 17
- 4.1 Conductor-like shielding model 18

5 Results and discussion 20
- 5.1 Model geometries 20
- 5.2 Mulliken charges 23
- 5.3 Hydration enthalpy 27
  - 5.3.1 Calculation of binding energy, ΔE_{b} 27
  - 5.3.2 Calculation of solvation energy, ΔE_{sol} 29
  - 5.3.3 Calculation of hydration enthalpy, $\Delta H^{\circ}_{\mathrm{hyd}}$ 30
- 5.4 Redox potentials 32
  - 5.4.1 Calculation of redox potentials 35
  - 5.4.2 Co^{3+}/Co^{2+} and Ni^{3+}/Ni^{2+} 37
  - 5.4.3 The reorganization energy 40
  - 5.4.4 Calculation of redox potentials of MOH^{2+}, H^{+}/M^{2+} . . . 42

6 Conclusions 44

Abstract 45

Kokkuvõte 46

References 47

Articles 52

Curriculum Vitae **78**

Elulookirjeldus **79!!**

List of publications

I M. Uudsemaa and T. Tamm, Calculations of hydrated titanium ion complexes: structure and influence of the first two coordination spheres. Chemical Physics Letters, **2001**, *342*, 667-672.

II M. Uudsemaa and T. Tamm, Density-functional theory calculations of aqueous redox potentials of fourth-period transition metals. Journal of Physical Chemistry A, **2003**, *107*, 9997-10003.

III M. Uudsemaa and T. Tamm, Calculation of hydration enthalpies of aqueous transition metal cations using two coordination spheres and central ion substitution. Chemical Physics Letters, **2004**, *400*, 54-58.

Abbreviations

BP86 — Becke-Perdew 86 exchange-correlation functional
COSMO — Conductor-like screening model, continuum model
DFT — Density Functional Theory
GGA — Generalized gradient approximation
HF — Hartree-Fock
LDA — Local density approximation
MO — Molecular orbital
QM/MM — Quantum mechanical/molecular mechanical
RI — Resolution of identity
SHE — Standard hydrogen electrode
SV(P) — Split-valence basis sets with polarization functions on non-hydrogen atoms
TZVPP — Triple-zeta valence quality basis sets augmented with double polarization functions
ZPE — Zero-point energy
λ — Reorganization energy

Introduction

Physical chemistry of aqueous solutions and ion hydration is one part of the inorganic and physical chemistry. The solvation structure around the metal ion is very important for quantitative interpretation of the equilibrium and chemical reactions concerning the metal ion. Much of the chemistry of the aqua ions is representative of the general chemical properties of the metal ion and the oxidation state.[1]

Many experimental studies using Raman spectroscopy have been carried out to describe the hydration (solvation) structure of nearly all stable metal ions.[2–7] For the first-row transition metal ions it is accepted that the hydration structure is octahedral six-coordinate.[1,8,9]

Various transition metal hexa-aqua ions have been investigated with quantum mechanical methods.[10–15] These calculations have reproduced experimental results in metal-oxygen distances or hydration enthalpies.

Electron transfer reactions are essential in chemistry and biology. The driving force for the electron transfer can be determined from the reduction potentials.[16] Some research groups have calculated the standard redox potentials in solution.[13,17–27] A general idea in these studies is to use a theoretical method to compute the gas-phase ionization energies and then to add the solvation energy terms calculated via the use of a solvation model.

This thesis comprises a computational work on the solvated first-row transition metals (Sc, Ti, V, Cr, Mn, Fe, Co, Ni, Cu) di- and trivalent ions, which has enabled a systematic comparison of the computational and the experimental data. Molecular properties such as hydration enthalpies and redox potentials, are calculated using the same gas phase and the solution energetic data. Also there are some predictions for the values of hydration enthalpies of Ni^{3+} and Cu^{3+} ions, where the experimental data do not appear to be determined.

Acknowledgements

This work was conducted in the Department of Chemistry of the Faculty of Science at Tallinn University of Technology.

I am grateful to my supervisor Toomas Tamm who has been supervising me for all these years that I have worked on this scientific field.

I which to thank my close co-workers Kaie Laane and Marina Kudrjashova for smooth collaboration and all kind of help. I am grateful to my colleagues and friends who have supported me during these years.

In addition, I would like to thank my family and parents for their love, patience, understanding and support during all these years.

This work was financially supported by Estonian Ministry of Education and Research, projects No. SF0142079s02, and the Estonian Science Foundation, Grant No. 3663. This work has also received network support from Nordisk Forskerakademi, NorFa Grant No. 030262.

1 Review of literature

1.1 Hydration enthalpy

Many chemical and biological reactions occur in water. In aqueous solution metal ions are strongly influenced by the hydration of the ions by the polar water molecules. The hydration energy represents the enthalpy change that accompanies the dissolving of 1 mol of gaseous ions in water,[1]

$$\mathrm{M}^{m+}(g) + n\mathrm{H_2O}(l) \xrightarrow{\Delta H^\circ_{\text{hyd}}} \mathrm{M}^{m+}(aq)(l) \tag{1}$$

A considerable number of computer simulations of aqueous solutions of ions have been reported. Only a limited number of solvent molecules can be included explicitly due to the high cost of the calculations. In the most common cases, for example Ichieda et al[28] and Asthagiri et al,[29] have quantum-chemically described only the first solvation sphere, water molecules around a ion. Some researchers[13,30–41] have, however, included also the second solvation sphere and have found such inclusion relevant for increasing the accuracy of description of energetic and spectroscopic effects.

Li et al[13] have found that for the divalent iron and manganese cations the first hydration shell model images the experimental hydration enthalpy measurements very well. For the trivalent cations the calculated hydration enthalpy was closer to the experimental results when the second solvation sphere (6 water molecules in the first sphere and 12 in the second sphere) was also included.

Using ab initio calculations at the MP2 level, Martinez et al[41] have compared the calculated hydration free energies for the second row transition metal ion $[\mathrm{Ag(H_2O)_4}]^+$ and $[\mathrm{Ag(H_2O)_{12}}]^+$ and have found that the difference between the experimental and calculated values increased, when the second solvation sphere (4 + 8) was included. Rudolph et al[31–34] have reported the calculated enthalpies for $\mathrm{Cd^{2+}}$, $\mathrm{Zn^{2+}}$, $\mathrm{Sc^{3+}}$ and $\mathrm{Al^{3+}}$ with confirmation of the importance of the second sphere.

1.2 Redox potentials

An electrochemical cell consists of two electrodes, or metallic conductors, in contact with an electrolyte, an ionic conductor which may be a solution, a liquid, or a solid.[16] The half redox reaction of the electrode reactions:[16]

$$\mathrm{M}^{(z+n)+}(aq) + n\mathrm{e}^- \longrightarrow \mathrm{M}^{z+}(aq) \tag{2}$$

describes the situation where both ions are in the solution. All aqueous compounds are at 1M concentration.

Redox potentials for a single electrode is not possible to measure. The potential of one of the electrodes can define as having zero potential and then assign values to others on that basis.[16] The standard redox potentials, E°, in aqueous solution are referred to the standard hydrogen electrode SHE. The SHE consists of hydrogen ion activity of 1 under the standard thermodynamic conditions, at 25 °C and 1 atm. The SHE half-reaction is:

$$1/2\mathrm{H}_2(g) \longrightarrow e^-(g) + \mathrm{H}^+(aq) \tag{3}$$

E°_{SHE} is declared to be zero. Reiss et al[42] have estimated the absolute ΔE°_{SHE} of -4.43 eV. This value is affirmed by theoretical and experimental works.

Lewis et al[43] have calculated the SHE free energy change 420.6 kJ/mol. The free energy change for eq 3 corresponds to an absolute potential. At standard conditions,

$$\Delta E^\circ_{SHE} = -\frac{\Delta G^\circ}{nF} \tag{4}$$

where ΔG° is the free energy change, n is the number of electrons transfered in the half-reaction and F is the Faraday constant. The value of ΔE°_{SHE}, according to eq 4, is –4.36 eV.[43]

1.2.1 Computational electrochemistry

Computational electrochemistry is an expanding field in computational chemistry. The pioneering work in this area are studies of the electrode potential by Liester et al[17] and by Li et al.[13] Liester et al studied the potential of 2,3-dicyanobenzoquione and Li et al calculated the redox potentials for the $\mathrm{Mn}^{3+}/\mathrm{Mn}^{2+}$ and $\mathrm{Fe}^{3+}/\mathrm{Fe}^{2+}$ pairs.

Several groups[18–20] have recently published papers on calculations of the redox couples using ab initio methods. A few studies have appeared in the literature that utilize Density Functional Theory (DFT) for computing the redox potentials in solutions. Baik et al have calculated the potential for small organic molecules, metallocenes and $\mathrm{M(bpy)}_3^x$ (M = Fe, Ru, Os; x = +3, +2, +1, 0, -1)[21] and cyclooctatetraene and nitrobenzene.[22] Fu et al[23] have developed a generally applicable protocol that could predict the standard redox potentials of 270 structurally unrelated organic molecules in acetonitrile. Dutton et al[24] have described computational predictions of the reduction potentials of reactive nitrogen oxides. Bachmann et al[25] have made DFT computations of the redox states of the iron porphyrinogens. Kobayashi et al[26] have evaluated the standard redox potential for the several metal/metal cation systems, Blumberger et al[27] have calculated the potential for $\mathrm{Cu}^{2+}/\mathrm{Cu}^+$ and $\mathrm{Ag}^{2+}/\mathrm{Ag}^+$. However, the common computational approach, based on quantum theory, for prediction of aqueous redox potentials of transition metals is rare in use.

2 Aims of the study

Computational studies of the metal ion-water complexes with the primary shell water molecules and the studies on water exchange mechanisms in the first coordination sphere were most common in this area several years ago. Development of the computing power gives more possibilities for the calculations. The number of studies of the aquated metal complexes with explicit inclusion of the second coordination sphere is on the increase.

In this thesis solvated di- and trivalent first row transition metal ions are regarded. The particular aims of this study were the following:

A. to test essentiality of the second (and the third) solvation shell in the supermolecule approach;

B. to compare two different approaches for the calculation of solvation energy, when the open-shell central ion is replaced by similarly-charged closed-shell species;

C. to calculate hydration enthalpies for the first row transition metal ions;

D. to calculate the aqueous redox potentials of the transition metals, M^{3+}/M^{2+} (M = Sc — Cu), and to compare with the experimental values to assess the accuracy of the methodology;

E. to study more precisely the less accurately calculated redox pairs;

F. to test the procedure of the calculations of aqueous redox potentials for the redox systems $MOH^{2+}, H^{+}/M^{2+}$ (M = Cr, Fe).

3 Theoretical background

3.1 Quantum chemical methods

Quantum chemistry calculations are based on the laws of quantum mechanics where the starting point is the time-independent Schrödinger equation

$$\hat{H}\Psi = E\Psi \tag{5}$$

where $\hat{H}$ is the Hamiltonian for the system , Ψ is the wave function and E is the energy. The traditional methods for the determination of the electronic structure are based on the many-electron wave function.

The Hartree-Fock (HF) method breaks the many-electron equation into many simpler one-electron equations. The restricted HF method (RHF) treats systems with singlet spin.[44] The electrons of α spin are forced to occupy the same spatial orbitals as those of β spin.

The unrestricted HF method (UHF) method separates spatial orbitals for the α and for the β electrons, giving two sets of molecular orbitals, one for α and one for the β electrons. The UHF wave function is used for open-shell states. The disadvantage of the UHF method is that the wave function is no longer an eigenfunction of the total spin operator. This error is called spin contamination. A high spin contamination can affect the geometry and population analysis and significantly affect the spin density.[45]

The restricted open-shell HF method (ROHF) constructs wave functions for open-shell molecules in another way. Electrons occupy molecular orbitals in pairs as in the RHF method, except for the unpaired electron(s).[45] The ROHF technique is more difficult to implement than the UHF. ROHF is primarily used for cases where spin contamination is large using the UHF method.[44]

Density Functional Theory (DFT) is one of the most popular techniques for calculating the electronic structure and it is widely used for the studying of the large systems such as metals and large molecules. In DFT, the energy of a molecule is determined from the electron density, it is only a function of three variables and by this way the building of the many-body wave function what is dependent on $3N$variables could be avoided.[45]

A practical application of DFT theory was developed by Kohn and Sham.[46] The density is expanded in a basis of molecular orbitals, similar to HF equations. A density functional is a function of the electron density function. The exact density functional is not known, therefore a lot of different functionals are constructed.

For the simplest functionals the energy depends only on the charge density ϱ at any given point in space, which leads to the local density approximation (LDA). Such functionals are computationally very fast, but tend towards systematic errors such as overestimating the bond dissociation energies and are no longer used intensively.

The electron density in an atom or molecule varies greatly from place to place.[45] The generalized gradient approximation (GGA) use exchange-correlation energy functionals E_{xc}, where the energy depends the electron density and the density gradient $\nabla\varrho$ (how fast it changes in space). The exchange-correlation energy functional can be written as the sum of an exchange-energy functional and a correlation-energy functional[45]

$$E_{xc} = E_x + E_c \tag{6}$$

These functionals can give the remarkably accurate results and are still computationally very efficient. Some of the most popular GGA functionals are the Becke-88 (B88)[47] exchange functional and the Lee-Yang-Parr (LYP)[48] and Perdew-86 (P86)[49] correlation functionals.

Hybrid functionals contain a mixture of the exact (i.e., HF) and DFT exchange. The hybrid DFT methods are the most accurate of the three classes. Of this type, the Becke three-parameter exchange functional (B3)[50] is the most common.

Last, there are the meta-GGA functionals (LAP3, Becke00) where the energies depend also on the Laplacian of the density $\nabla^2\varrho$ and/or the orbital kinetic energy.

The DFT functionals typically have exchange and correlation parts that are constructed independently. In this work we have used the Becke-Perdew 86 (BP86) exchange-correlation functional as implemented in the Turbomole package.

3.2 Solvent effects

Solvent effects could be classified as follows:

1. Specific solvation (e.g. hydrogen bonds);
2. Non-specific solvation (usually applied as a polar medium, the presence of an implicit solvent environment as a continuum).

Specific solvation depends strongly on particular features of the solute and the solvent. Water molecules that will be in the direct contact with the ion constitute the primary hydration shell. The water molecules outside the shell have different properties from the bulk water due to a transmitted effect though the hydrogen bonding with the first coordination shell.[1] This is called the second coordination shell.

The most relevant chemically bounded parts are modeled quantum-chemically in a cluster calculations. The cluster is formed from the molecules of a solvent with molecules or ions of a solute. The quantity of the solvent molecules in the first hydration shell is the same as the ion coordination number.

The model can be improved by adding a second solvation sphere to it. If the coordination number is not known, it must be determined by adding extra solvent molecules to the first solvation sphere or the second solvation sphere in order to test which one is the most stable.[51] Several QM/MM simulations[38–40] have indicated that the the second coordination shell could contain 12-16 water molecules. Some DFT studies[7,13] have found that about 12 water molecules are required to compile the second solvation sphere around primarily hydrated di- and trivalent ions of the first row transition metals.

Non-specific solvation is represented by the continuum models. The molecule is surrounded by the virtual charges that polarize it as a surrounding solvent. These charges are situated on the surface of an imaginary cavity in a solvent. Two the most used continuum models are the polarisable continuum model (PCM)[52] and the conductor-like shielding model (COSMO)[53] (see Section 4.1).

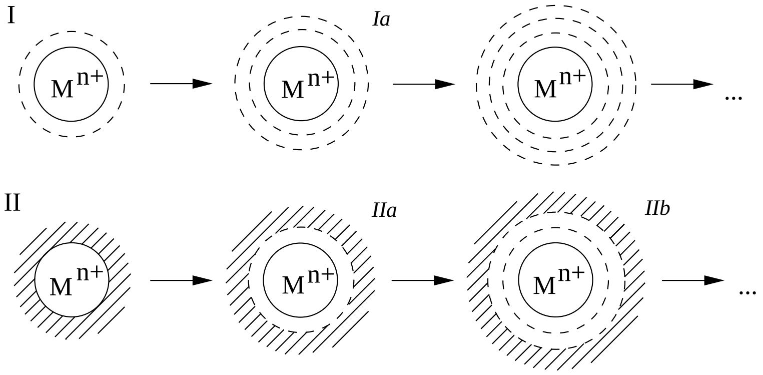

Figure 1: Schematic depiction of the solvation of an ion M^{n+}

Two approaches to describe solvation of an ion M^{n+} are represented in Figure 1.[54] The ion is always described quantum-mechanically. In the first (I), supermolecule approach, solvent molecules (represented by dashes) are included in to the quantum-mechanical model. The model would be more accurate by accounting for an increasing number of solvent shells. These clusters may or may not be a good approximation to the real description of the metal ion in a solution.[51]

The second approach (II) shown in Figure 1 takes the long-range electrostatic interactions into account via a continuum model. Hybrid supermolecule-continuum models (*IIa*, *IIb*) have proved to be useful in different quantum-chemical calculations.[13,28–41]

Some expression used in literature shall be introduced to in conclusion. There are two different expressions for the ion-water cluster: the coordination sphere and the solvation sphere. One possibility to describe a cluster *Ia* in Figure 1 is the following: the metal ion, the first coordination sphere, and the first solvation sphere. Another way is to enumerate the metal ion surrounded by the first and the second coordination shells[55] or hydration[13] or solvation spheres (ligands).[56] In this thesis the first and the second (and the third) solvation spheres are used for depiction the cluster.

3.3 Crystal field theory

Crystal field theory was the first systematic approach for the explanation of the properties of complexes. It is based on a model in which the effect of the ligands is treated as an essentially ionic problem. In the crystal field theory, each ligand is represented by a negative point charge.[57]

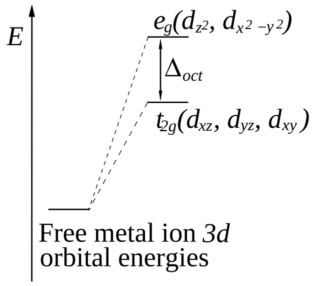

Figure 2: The energies of the *3d* orbitals for a metal ion in an octahedral complex

Whereas in a free atom all five d orbitals have the same energy d-orbitals split into two different energy levels in an octahedral crystal field (Figure 2),[57] d_{xy}, d_{xz}, d_{yz} (labeled t_{2g}) and d_{z2}, d_{x2-y2} (labeled e_g). The electrons around the ligands will interact strongly with the electrons in the two orbitals that are aligned along the axes (d_{z2} and d_{x2-y2}) and less strongly with the electrons in the other three orbitals (Figure 3).[57] These interactions cause the energies of electrons in these orbitals to split.

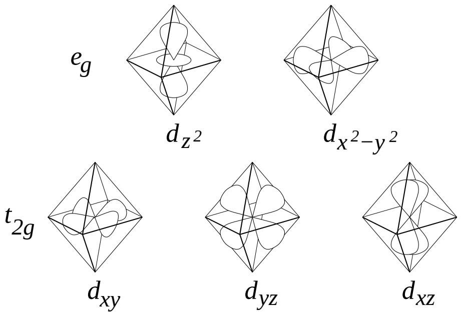

Figure 3: The *3d* orbitals for a metal ion in an octahedral complex

The energy gap between them is called the ligand field splitting energy (Δ_{oct}).[1,57] Pairing energy (P) is required to pair up electrons within the same orbital, the energy needed to overcome the extra repulsion from electrons residing in the same orbital. The values of the Δ_{oct} and P explain the origin of the high-

and the low-spin forms.[1] If the value of Δ_{oct} exceeds this pairing energy then a low-spin complex will be the result. If $P > \Delta_{oct}$ the high-spin complex according Hund's rule will be formed: every orbital in a subshell is singly occupied with one electron before any one orbital is doubly occupied. In the low-spin case Δ_{oct} is too large to set electrons in the high energy orbitals and they occupy in the lower levels in pairs.

4 Computational aspects

For calculations of the energetic parameters the triple-zeta valence quality basis sets augmented with double polarization functions (TZVPP)[58] were used. As part of the work done for my Master's thesis[59] I compared split valence (SV), double-zeta (DZ) and triple-zeta (TZV) basis sets. Reasonable convergences of the binding energies was achieved with the TZVPP basis set for the studied transition metal systems.

The resolution of identity (RI)[60] technique increases the efficiency of DFT calculations.[61,62] Products of basis functions $\nu(r)\mu(r)$, are approximated by a linear expansion of so-called auxiliary basis functions, *P(r)*,[63]

$$\nu(r)\mu(n) \approx \sum_i c^P_{\nu\mu} P_i(r) \tag{7}$$

Here basis functions are linearly combined to describe molecular orbitals. Minimizing the self-interaction of the error in the expansion leads to an approximation for two electron integrals:[64]

$$(\nu\mu|k\lambda) \approx \sum_{P,Q} (\nu\mu|P)(P|Q)^{-1}(Q|k\lambda) \tag{8}$$

The orbitals associated with electron 1 can swap with those associated with electron 2. In total, two-electron integrals over spatial orbitals have eightfold symmetry.

$$\begin{aligned}
(\nu\mu|k\lambda) &= (\mu\nu|k\lambda) \\
&= (\nu\mu|\lambda k) \\
&= (\mu\nu|\lambda k) \\
&= (k\lambda|\nu\mu) \\
&= (\lambda k|\nu\mu) \\
&= (k\lambda|\mu\nu) \\
&= (\lambda k|\mu\nu)
\end{aligned} \tag{9}$$

For two-electron integrals, the eightfold symmetry means that only about one in eight two-electron integrals are unique and must be stored. The others can be accessed by permutations of the orbital labels. Efficiency and accuracy of RI do not depend on a molecule's geometric and electronic structure and size.[63]

In this work RI technique was used to speed up the calculations. It was used in optimizations of the systems containing 18 or 42 water molecules. We have used the auxiliary basis functions provided with the Turbomole package.

Non-hybrid BP86 functional was chosen according to the requirement for the RI technique. Although the hybrid DFT methods, especially B3LYP, are estimated to be more accurate, recent studies of the transition metal complexes suggest that it may not be the best choice for these systems.[51] Also the RI technique is not available for the B3LYP functional in Turbomole version 5.5 and 5.6.

Energetic estimates for the clusters with the optimized geometries were obtained without using the RI approximation as single point calculations. The difference between RI and non–RI technique were $\sim$ 5 kJ/mol for systems with 18 water molecules. RI technique was not necessary for the systems with six water molecules, the appropriate calculations have been made directly.

Minima were confirmed by the vibrational analysis. For the systems containing 6 water molecules the vibrational analysis was done at the TZVPP level. For other systems this check was executed at a smaller– split-valence basis with the polarization functions on the non-hydrogen atoms – the SV(P)[65] level, with the SV(P)-optimized geometry. It was assumed that the validation of minima at the SV(P) level was sufficient – vibrational calculations with a larger basis (TZVPP) would have been too time-consuming, at the same time the difference between the calculated zero-point energies was not very big, $\sim$ 0.5 kJ/mol for a trial system. The time for the TZVPP calculation, however, increased up to 7-8 times, from a few days to three weeks.

A molecule (a cluster) always has some vibrational motion. Zero-point energy (ZPE) is the energy difference between the minimum on a potential energy surface and the first vibrational energy level.[44] For the BP86 calculations the ZPE were calculated from vibrational analysis and the energies were added to the calculated energies of all systems for getting the total energy of the system.

4.1 Conductor-like shielding model

The conductor-like shielding model (COSMO)[53] was developed by Klamt and co-workers. This model calculates the dielectric screening charges and energies on a van der Waals-like molecular surface in the approximation of a conductor observed on a molecular cavity. This simplifies the electrostatics computations, and corrections are made a posteriori for dielectric behavior.[66]

The surface of the molecules is considered to be a collection of equally sized surface segments. The surface charge density should be homogeneous within a segment.[67]

The surface charge distribution gives rise to an electric field, with which the solute charge density then interacts. The total electrostatic energy of this system is the sum of the solute-surface interaction and the surface self-interaction,[68]

$$G_{diel}^{cond}[\sigma] = \int_v d^3r \int_s d^2s \frac{\rho(r)\sigma(s)}{|r-s|} + \frac{1}{2}\int_s d^2s \int_s d^2s' \frac{\sigma(s)\sigma(s')}{|s-s'|} \tag{10}$$

where ρ(r) is the total charge density of the solute, and σ(s) is the surface charge distribution.

The polarization induced by the solute charge density is represented by a surface charge distribution on the cavity boundary. The boundary condition at the solute/solvent interface is matched the solute and the solvent electric field. The polarisability of the continuum is governed by its dielectric constant, ϵ. The surface charges are determined by scaling the screening conductor surface charge by a factor[53]

$$f(\epsilon) = \frac{\epsilon - 1}{\epsilon + \frac{1}{2}} \tag{11}$$

The variational energy expression including dielectric scaling:[68]

$$G_{diel}^{COSMO}[\bar{\sigma}] = \int_v d^3r \int_s d^2s \frac{\rho(r)\bar{\sigma}(s)}{|r-s|} + \frac{1}{2f}\int_s d^2s \int_s d^2s' \frac{\bar{\sigma}(s)\bar{\sigma}(s')}{|s-s'|} \tag{12}$$

where $\bar{\sigma}$(s) denotes the scaled surface change.

The surface charge distribution $\bar{\sigma}$(s) is correspondingly approximated by discrete (scaled) surface charges, q_i, located at the center of each segment. The energy can be written as:[68]

$$G_{diel}^{COSMO}(\{q_i\}) = E^{s--m} + E^{s--s} + E^{self} \tag{13}$$

Here E^{s--m} denotes the interaction between the segments and the solute molecule. The self-interaction of the surface charge distribution has been split into two terms; The segment-segment interaction E^{s--s}, and the segment self-interaction E^{self}.

Conductor-like model is highly accurate and more efficient compared to the solution of the dielectric boundary conditions.[67] In this thesis we have used the continuum model COSMO as implemented in the Turbomole package. The dielectric constant of water at 25°C (78.5) was used. For the cavity construction in the COSMO calculations, the default atomic radii of the Turbomole package were used.

5 Results and discussion

The studies for this thesis cover two test of the relevance of the second (and third) solvation shell in the supermolecule approach. At first, hydration enthalpies for the fourth-period transition metal ions Sc, Ti, V, Cr, Mn, Fe, Co, Ni, Cu, with charges 2+ and 3+ have been calculated. Secondly, the aqueous redox potentials of the M^{2+}/M^{3+} ions (M = Sc — Cu) and MOH^{2+}, H^{+}/M^{2+} (M = Cr, Fe) have been calculated. The fourth-period transition metal ions were chosen to reduce the need to account for relativistic effects that will become increasingly prominent in the subsequent periods. Experimental data were used as a reference, and to validate the computational results.

5.1 Model geometries

Typically the first row transition metal di- and trivalent ions have the coordination number of six.[1,8] In a quantum chemical model the six water molecules are in a direct contact with an ion, forming the first coordination shell of the 6-water cation complex (Figure 4).

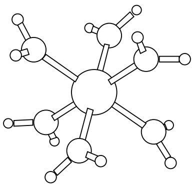

Figure 4: Structure of the six-water model cation complex, $[M(H_2O)_6]^{n+}$

Complexes with different symmetries were compared to find the lowest energy. Three local minima with the C_i, S_6 and T_h symmetry were located. The symmetries are in good agreement with results of the earlier similar studies.[10,14]

Also the spin state of the system was controlled, optimizations with all possible spin states were carried out. The multiplicity is verified by comparing energies of the complexes. The lowest energy indicates the system's low- or high-spin state.

In order to introduce the second solvation sphere we have attached a hydrogen bonded water molecule to each hydrogen atom of the first sphere, yielding the 18-water cation complex. Several local minima were located. In our articles I and II we have taken a look at two different minima for this complex. In this thesis have originated from the lowest energy configurations (Figure 5) for ion — 18 water molecules complexes.

It is considered that the "wheel–like" configuration (Figure 5) could be the global minimum.[69,70] The bond lengths in the complexes with one and two coordination sphere were compared. Adding the second coordination sphere leads to

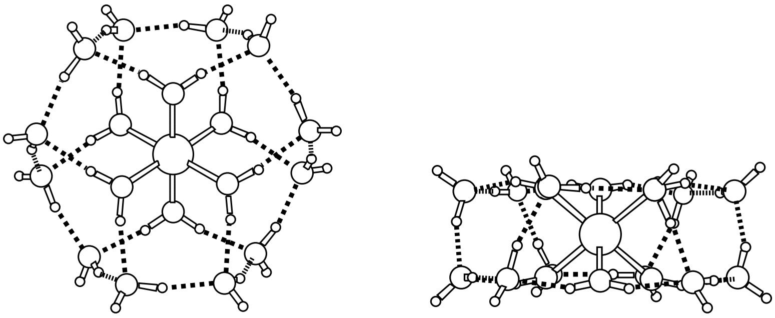

top view side view

Figure 5: Structure of the 18-water model cation complex, $[M(H_2O)_{18}]^{n+}$

the shorter ion–oxygen bond lengths[69,70,I]. It is appointed that the inner solvation sphere adopts a near-D_{3d} all-horizontal symmetry[69,70,I].

A further highly diffuse region, the third coordination shell, may be present before the distances are reached so far from the ion that the water molecules become essentially indistinguishable from those of bulk water.[1] The importance of the third coordination shell is inquired. The third shell is modeled, to each water molecule in the second shell were attached two more water molecules, yielding the 42-water cation complex.

The cluster with three explicitly-modeled solvation spheres is computationally expensive. The time for the geometry optimization at the TZVPP level, originating from SV(P) optimized geometry systems, with 18 water molecules and systems with 42 water molecules, is increasing from 4 days to 16 days.

In this study the calculation of the third coordination shell was made only for the iron di- and trivalent ions. The complexes with iron as central ion was chosen because the experimentally measured Fe^{3+}/Fe^{2+} potential at -0.771 V is confirmed by two measurements[71,72] and our previous calculations[II] has reproduced the value difference of -0.04 V. Also in the hydration enthalpy calculations[III] the complexes with iron cations have shown good accuracy.

Two different local minima are located (Figure 6, 7). The inner solvation sphere adopts a near-C_i symmetry.

The cluster may be not a good approximation for the real situation of the metal ion in solution. The more atoms are included in a system, the larger's the number of degrees of freedom and the higher is the number of likely minimum energy structures. The real system is more dynamic, furthermore, using a polarisable continuum it is possible to simulate the time-averaged water molecules that surround the cluster in a solution.[51]

The optimized M–O distances in $[Fe(H_2O)_n]^{m+}$ (n = 6, 18, 42; m = 2, 3) and the available experimental data are summarized in Table 1 p. 23. Adding

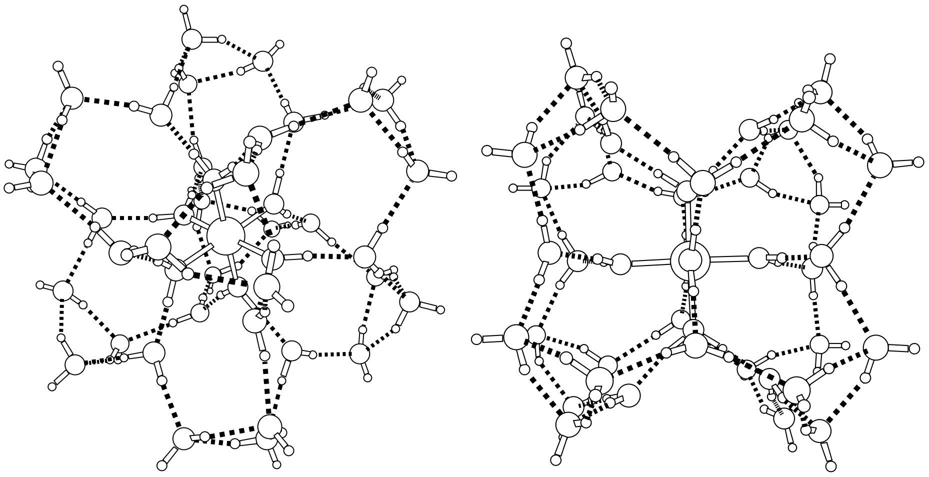

top view side view

Figure 6: Structure *A* of the 42-water model cation complex, $[M(H_2O)_{42}]^{n+}$

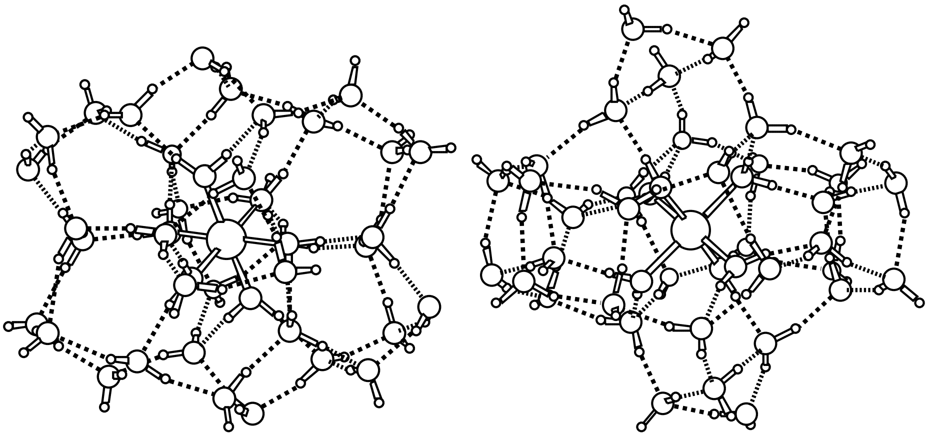

top view side view

Figure 7: Structure *B* of the 42-water model cation complex, $[M(H_2O)_{42}]^{n+}$

the second solvation shell to the Fe^{2+} ion did not modify the ion–oxygen bond lengths. The same held also for the third shell. For Fe^{3+} the second solvation sphere is more essential, the calculated ion–oxygen bond lengths are in a better agreement with the experimental values than in the $[Fe(H_2O)_6]^{3+}$ cluster. Adding the third shell did not reduce the lengths significantly.

Formation of hydrogen bonds between water molecules is mostly compen-

Table 1: M - O distances in [Fe(H_2O)$_n$]$^{m+}$, in Å

	Ion				
Ion	+6 H_2O	+18 H_2O	+42 H_2O (*A*)	+42 H_2O (*B*)	Expt.[73]
Fe^{2+}	2.13...2.17	2.13...2.15	2.12...2.17	2.13...2.14	2.095-2.28
Fe^{3+}	2.07	2.04	2.04	2.02...2.05	1.99-2.05

sating, causing changes in enthalpy (becoming more negative) and entropy (becoming less positive). This enthalpy-entropy compensation is almost complete, however, with the consequence that very small imposed enthalpic or entropic effects may exert a considerable influence on aqueous systems.

The number of hydrogen bonds in type *A* structure is 55, in type *B* structure is 64. For the Fe^{2+} and Fe^{3+} central ions the complex *B* (Figure 7) has the lower energy 164 and 88 kJ/mol, respectively. It is similar with previously studied^{II} [M(H_2O)$_{18}$]$^{m+}$, (M= Sc — Cu; m = 2, 3) complexes, where the system with more hydrogen bonds (Figure 5) had the lower energy.

5.2 Mulliken charges

One of the most immediate properties of a molecule or a cluster is its charge. Assigning atomic charges and bond orders involves calculating the number of electrons belonging to an atom or shared between atoms. There is no unique definition of how many electrons are attached to an atom in a molecule (or in a cluster).

One of the widely used population analysis schemes is the Mulliken population analysis. Each molecular orbital has a wave function ψ:[45]

$$\psi_m = c_{1m}\phi_1 + c_{2m}\phi_2 + c_{3m}\phi_3 + ... + c_{mm}\phi_m \tag{14}$$

Here the basis set ϕ_1, ϕ_2, ... , ϕ_m engenders molecular orbitals (MO) ψ_1, ψ_2, ... , ψ_m. c_{si} is the coefficient of basis function *s* in MO *i*. For any MO ψ_i, squaring and integrating over all space gives[45]

$$\begin{aligned} \int |\psi_i|^2 dv &= 1 \\ &= c_{1i}c_{1i}S_{11} + c_{2i}c_{2i}S_{22} + ... \\ &\quad +2c_{1i}c_{2i}S_{12} + +2c_{1i}c_{3i}S_{13} + 2c_{2i}c_{3i}S_{23} + ... \end{aligned} \tag{15}$$

The integral equals one because the probability that the electron is somewhere in the MO is one. The basis functions are normalized, S_{ii} are the overlap integrals, where both basis functions ϕ are the same. The square of a molecular orbital gives many terms, some of which are the square of a basis function (e.g. $c_{ri}c_{ri}S_{rr} = c^2_{ri}$) and others are products of basis function (e.g. $2c_{ri}c_{si}S_{rs}$), which yield the ψ_r/ψ_s overlap when integrated. Thus, the orbital integral is actually a sum of integrals over one or two center basis functions.[44]

If there are n_i electrons in MO ψ_i, then the contributions of ψ_i to the electron population of basis function ϕ_i and of the overlap region between ψ_r and ψ_s are:[44]

$$n_{r,i} = n_i c^2_{ri} \tag{16}$$

$$n_{r/s,i} = n_i(2c_{ri}c_{si}S_{rs}) \tag{17}$$

In Mulliken analysis the contribution of a basis function in all orbitals is summed to give the net population n_r of that basis function. The overlaps for a given pair of basis functions $n_{r/s}$ are summed for all orbitals in oder to determine the overlap population for that pair of basis functions.[44] The Mulliken gross population in the basis function ϕ_r is defined:[45]

$$N_r = n_r + \frac{1}{2}\sum_{s\neq r} n_{r/s} \tag{18}$$

The gross population N_r is an attempt to represent the total electron population in the basis function ϕ_r.

The Mulliken approach to population analysis has certain problems. For example it sometimes assigns more than two electrons, and sometimes a negative number of electrons, to an orbital. It is also fairly basis-set dependent.[45] For the large basis sets, results can be very unreasonable. The charge is more diffused with the TZVPP basis than with the SV(P) one in our calculations for the first row transition metal ions. Some example are shown in Table 2.

Table 2: Mulliken population analysis

	SV(P)			TZVPP		
Complex	Central ion	First solvation sphere	Second solvation sphere	Central ion	First solvation sphere	Second solvation sphere
$[Fe(H_2O)_{18}]^{2+}$	0.82	0.13	1.05	0.82	0.50	0.68
$[Cu(H_2O)_{18}]^{2+}$	0.68	0.23	1.09	0.46	0.81	0.73
$[Fe(H_2O)_{18}]^{3+}$	1.01	0.51	1.49	0.76	1.06	1.18
$[Cu(H_2O)_{18}]^{3+}$	0.59	0.85	1.56	0.26	1.51	1.23

The studies gave different atomic charges, but there is nothing to indicate which of these gives the best result. In this study the Mulliken population analysis is performeded with a TZVPP basis set and results have been shown in Figure 8 and 9.

The electron density is clearly transfered from the surrounding medium to the central ion. In both cases, for charges 2+ and 3+, the charge of the central ion is almost constant for the complexes with one and two solvation shells. So, adding the second solvation sphere does not act on the ion. Except the charge of the central ion in the $[Cu(H_2O)_{18}]^{3+}$ complex, it is half as much as in the $[Cu(H_2O)_6]^{3+}$ complex.

With the addition of the outer solvation sphere, the positive charge tends towards dissipation on the surface of the charged “sphere”. In $[M(H_2O)_{18}]^{m+}$ (M = Sc — Cu; m = 2, 3) complexes the charge of the second solvation sphere is the same, without reference to the charge of the ion or the first solvation sphere.

The lone pairs on the oxygen atoms from the first coordination sphere have the co-ordinate bonds with a central ion. There is obviously a movement of electrons towards the ion. For $[M(H_2O)_6]^{m+}$ (M= Sc — Cu; m = 2, 3) complexes the oxygen in the first solvation sphere has a charge of –0.39...–0.42 for the divalent ions and –0.19...–0.41 for the trivalent ions. Each of the hydrogen atoms in the first sphere has a charge of 0.27 for the divalent ions and 0.31...0.32 for the trivalent ions.

For $[M(H_2O)_{18}]^{m+}$ (M= Sc — Cu; m = 2, 3) the oxygen in the first sphere is bearing the charge of –0.4...–0.48 for the divalent ions and -0.28...-0.52 for the trivalent ions. The charge of oxygen in the second sphere is –0.44 and –0.43, respectively. Each of the hydrogen atoms in the first and second sphere is bearing the charge of 0.25 for the divalent ions and 0.27 for the trivalent ions. The overall effect is that the charge, 2+ or 3+, is no longer located entirely on the metal ion but spreaded out over the whole cluster, much of it on the hydrogen atoms.

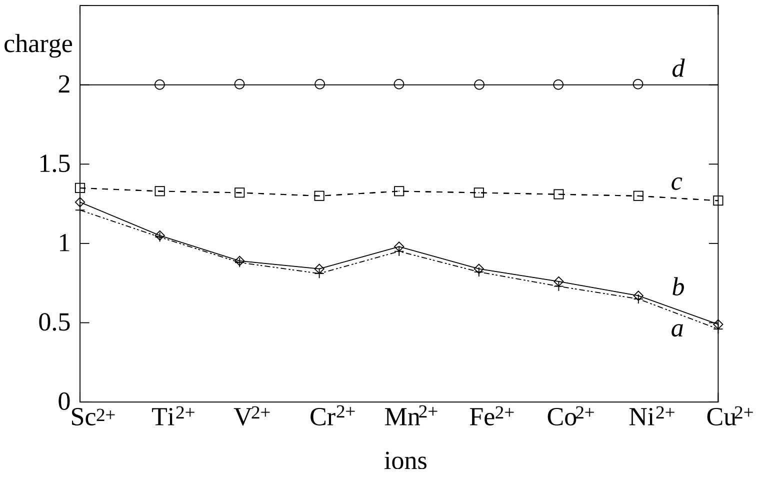

Figure 8: Mulliken charges for complexes $[M(H_2O)_6]^{2+}$
and $[M(H_2O)_{18}]^{2+}$, M= Sc — Cu

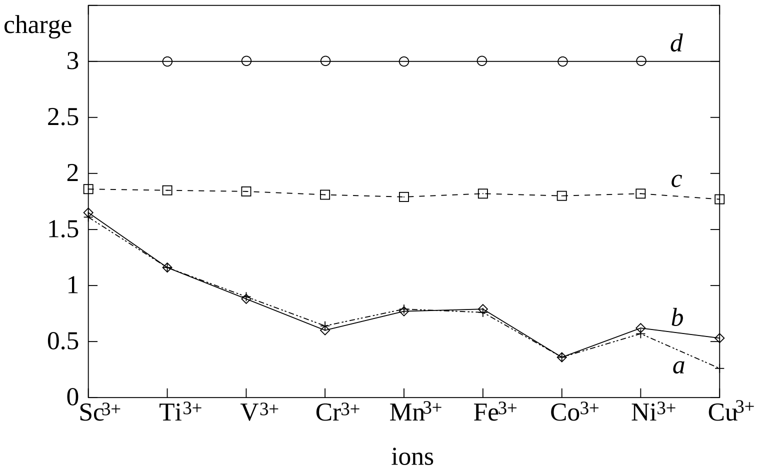

Figure 9: Mulliken charges for complexes $[M(H_2O)_6]^{3+}$
and $[M(H_2O)_{18}]^{3+}$, M= Sc — Cu

In Figure 8 and 9 lines:
a — the charge of the central ion in the $[M(H_2O)_{18}]^{m+}$ complexes;
b — the charge of the central ion in the $[M(H_2O)_6]^{m+}$ complexes;
c — the cumulative charge of the first solvation shell in the $[M(H_2O)_{18}]^{m+}$ complexes;
d — the cumulative charge of the first solvation shell in the $[M(H_2O)_6]^{m+}$ and the second solvation shell in the $[M(H_2O)_{18}]^{m+}$ complexes.

5.3 Hydration enthalpy

The energetics of formation of aqua complexes can be described by the enthalpy differences $\Delta H^\circ_{\text{hyd}}$ (hydration enthalpies). The calculation is based on the Born-Haber cycle shown in Figure 10.[15]

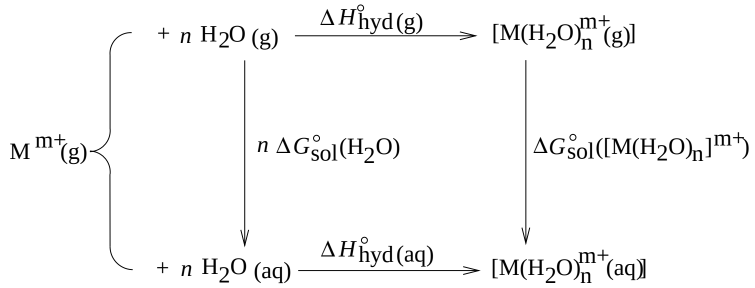
$+ \; n \; H_2O$ (g)
$\Delta H^\circ_{\text{hyd}}$ (g)
$[M(H_2O)_n^{m+}$ (g)]
M^{m+}(g)
$n \; \Delta G^\circ_{\text{sol}}(H_2O)$
$\Delta G^\circ_{\text{sol}}([M(H_2O)_n]^{m+})$
$+ \; n \; H_2O$ (aq)
$\Delta H^\circ_{\text{hyd}}$ (aq)
$[M(H_2O)_n^{m+}$ (aq)]

Figure 10: The thermodynamic cycle defining hydration $\Delta H^\circ_{\text{hyd}}$

Here Δ G°_{sol} represents the free energies of solvation and it can express as:

1. the heat of vaporization of water;
2. the transfer of gaseous $[M(H_2O)_n]^{m+}$ ions into bulk water without additional complex formation.

For calculation of hydration enthalpies we used the following equation:[13,15]

$$\Delta H^\circ_{\text{hyd}} = \Delta E_{\text{b}} + \Delta E_{\text{sol}} + n\Delta H_{\text{vap}} + \Delta nRT, \qquad (19)$$

here $\Delta H^\circ_{\text{hyd}}$ is the enthalpy of hydration, ΔE_{b} - the binding energy, ΔE_{sol} - the solvation energy of the cluster, ΔH_{vap} - the experimental heat of vaporization of water and Δn - the change in the number of molecules in the reaction. The values of ΔE_{b} and ΔE_{sol} have been calculated quantum-chemically.

5.3.1 Calculation of binding energy, ΔE_{b}

There are two different approaches for calculation of binding energy, ΔE_{b}, between the central ion and the cluster of water:[13,15,26]

$$\Delta E_{\text{b}}(\text{M—}n\text{H}_2\text{O}) = E[\text{M(H}_2\text{O)}_n^{m+}\text{(g)}] - E[\text{M}^{m+}\text{(g)}] - nE[\text{H}_2\text{O (g)}]; \qquad (20)$$

$$\Delta E_{\text{b}}(\text{M—}n\text{H}_2\text{O}) = E[\text{M(H}_2\text{O)}_n^{m+}\text{(g)}] - E[\text{M}^{m+}\text{(g)}] - E[(\text{H}_2\text{O})_n\text{(g)}], \qquad (21)$$

here $E[\text{M(H}_2\text{O)}_n^{m+}\text{(g)}]$ is the calculated energy of the system, $E[\text{M}^{m+}\text{(g)}]$ is the calculated energy of the central ion, and n is the number of water molecules (6 or 18). In all cases ZPE was included.

The difference between eq 20 and eq 21 applies to the energy of water molecules or cluster. In eq 20 the calculated energy of a single water molecule

$E[\mathrm{H_2O(\ g)}]$ multiplied on to the number of the water molecules *n* is used, in eq 21 the energy of a geometry-optimized water cluster $E[(\mathrm{H_2O})_n(\mathrm{g})]$ is used.

There is no common opinion for calculation of binding energy. Some researchers[13,15] have used the eq 20 and some[26] eq 21 in their work. We have calculated binding energies using both equations. Results are presented in Table 3.

Table 3: The calculated binding energies, in kJ/mol

Ion	eq 20	eq 21	Ion	eq 20	eq 21
$[\mathrm{Sc(H_2O)_6}]^{2+}$	-1090	-977	$[\mathrm{Sc(H_2O)_6}]^{3+}$	-2299	-2186
$[\mathrm{Sc(H_2O)_{18}}]^{2+}$	-1807	-1252	$[\mathrm{Sc(H_2O)_{18}}]^{3+}$	-3416	-2855
$[\mathrm{Ti(H_2O)_6}]^{2+}$	-1120	-1007	$[\mathrm{Ti(H_2O)_6}]^{3+}$	-2517	-2404
$[\mathrm{Ti(H_2O)_{18}}]^{2+}$	-1859	-1303	$[\mathrm{Ti(H_2O)_{18}}]^{3+}$	-3653	-3098
$[\mathrm{V(H_2O)_6}]^{2+}$	-1204	-1091	$[\mathrm{V(H_2O)_6}]^{3+}$	-2631	-2518
$[\mathrm{V(H_2O)_{18}}]^{2+}$	-1939	-1383	$[\mathrm{V(H_2O)_{18}}]^{3+}$	-3810	-3254
$[\mathrm{Cr(H_2O)_6}]^{2+}$	-1255	-1142	$[\mathrm{Cr(H_2O)_6}]^{3+}$	-2799	-2686
$[\mathrm{Cr(H_2O)_{18}}]^{2+}$	-1983	-1427	$[\mathrm{Cr(H_2O)_{18}}]^{3+}$	-3978	-3423
$[\mathrm{Mn(H_2O)_6}]^{2+}$	-1224	-1111	$[\mathrm{Mn(H_2O)_6}]^{3+}$	-2865	-2752
$[\mathrm{Mn(H_2O)_{18}}]^{2+}$	-1928	-1373	$[\mathrm{Mn(H_2O)_{18}}]^{3+}$	-4051	-3495
$[\mathrm{Fe(H_2O)_6}]^{2+}$	-1289	-1176	$[\mathrm{Fe(H_2O)_6}]^{3+}$	-2814	-2701
$[\mathrm{Fe(H_2O)_{18}}]^{2+}$	-2016	-1460	$[\mathrm{Fe(H_2O)_{18}}]^{3+}$	-3978	-3423
$[\mathrm{Co(H_2O)_6}]^{2+}$	-1334	-1221	$[\mathrm{Co(H_2O)_6}]^{3+}$	-3351	-3238
$[\mathrm{Co(H_2O)_{18}}]^{2+}$	-2068	-1512	$[\mathrm{Co(H_2O)_{18}}]^{3+}$	-4585	-4030
$[\mathrm{Ni(H_2O)_6}]^{2+}$	-1423	-1310	$[\mathrm{Ni(H_2O)_6}]^{3+}$	-3152	-3039
$[\mathrm{Ni(H_2O)_{18}}]^{2+}$	-2151	-1595	$[\mathrm{Ni(H_2O)_{18}}]^{3+}$	-4171	-3616
$[\mathrm{Cu(H_2O)_6}]^{2+}$	-1452	-1339	$[\mathrm{Cu(H_2O)_6}]^{3+}$	-3321	-3208
$[\mathrm{Cu(H_2O)_{18}}]^{2+}$	-2212	-1656	$[\mathrm{Cu(H_2O)_{18}}]^{3+}$	-4532	-3976

The differences between the calculated binding energies are 113 kJ/mol for $[\mathrm{M(H_2O)_6}]^{m+}$ and 555 kJ/mol for $[\mathrm{M(H_2O)_{18}}]^{m+}$ systems. In all cases eq 20 gives higher energies. It is caused by the energy discrepancies between $nE[\mathrm{H_2O\ (g)}]$ and $E[(\mathrm{H_2O})_n(\mathrm{g})]$. To avoid the supplementary errors (our water cluster could not depict water molecules in solution in the best way) we use eq 20 in this work.

5.3.2 Calculation of solvation energy, ΔE_{sol}

In some cases, the continuum solvation model can not be used for the open-shell systems. In some program packages for the electronic structure calculations the continuum solvent effect can be calculated only for the closed-shell systems. We faced this limitation in an earlier version (5.3) of the Turbomole package, where the open-shell calculations with the COSMO model were not implemented.

We constructed a model replacing an open shell central ion with a similarly-charged closed-shell species and calculated the solvation energy for the system^{III}. The central ions were replaced with Ca^{2+} or Sc^{3+} ion, respectively. Ca^{2+} or Sc^{3+} ions were chosen because they are the first closed-shell ions in the row. The geometry of the cluster was optimized in the gas phase with the correct central ion. Fixed geometry was used in the continuum calculations. Gas phase energy (single point calculation) for the modified cluster was found too.

With the implementation of the COSMO model for the open-shell systems in later versions (since Turbomole version 5.5), it became possible to test the validity of the approximation. The results are presented in Table 4.

Our approach and the direct open-shell COSMO calculations gave the similar results. The difference between the closed shell models and the true open shell systems was –3...+7 kJ/mol in most cases. The difference was larger for $[Fe(H_2O)_{18}]^{2+}$ and $[Ti(H_2O)_6]^{3+}$ complexes, where the closed shell systems yielded 13...14 kJ/mol lower energies than the open shell systems. Based on the present study, the central ion substitution can be recommend in cases where the open-shell continuum calculations can not be carried out directly.

Table 4: The calculated solvation energies, in kJ/mol

	Replaced	Correct		Replaced	Correct
Ion	central atom		Ion	central atom	
$[Sc(H_2O)_6]^{2+}$	-787	-781	$[Sc(H_2O)_6]^{3+}$	-1745	-1745
$[Sc(H_2O)_{18}]^{2+}$	-622	-618	$[Sc(H_2O)_{18}]^{3+}$	-1272	-1272
$[Ti(H_2O)_6]^{2+}$	-788	-787	$[Ti(H_2O)_6]^{3+}$	-1778	-1762
$[Ti(H_2O)_{18}]^{2+}$	-621	-620	$[Ti(H_2O)_{18}]^{3+}$	-1281	-1278
$[V(H_2O)_6]^{2+}$	-791	-790	$[V(H_2O)_6]^{3+}$	-1778	-1771
$[V(H_2O)_{18}]^{2+}$	-625	-626	$[V(H_2O)_{18}]^{3+}$	-1281	-1282
$[Cr(H_2O)_6]^{2+}$	-788	-791	$[Cr(H_2O)_6]^{3+}$	-1794	-1791
$[Cr(H_2O)_{18}]^{2+}$	-619	-619	$[Cr(H_2O)_{18}]^{3+}$	-1283	-1286

Table 4: (Continued)

Ion	eq 20	eq 21	Ion	eq 20	eq 21
$[Mn(H_2O)_6]^{2+}$	-786	-785	$[Mn(H_2O)_6]^{3+}$	-1783	-1784
$[Mn(H_2O)_{18}]^{2+}$	-620	-621	$[Mn(H_2O)_{18}]^{3+}$	-1280	-1282
$[Fe(H_2O)_6]^{2+}$	-793	-792	$[Fe(H_2O)_6]^{3+}$	-1774	-1772
$[Fe(H_2O)_{18}]^{2+}$	-635	-622	$[Fe(H_2O)_{18}]^{3+}$	-1284	-1280
$[Co(H_2O)_6]^{2+}$	-798	-797	$[Co(H_2O)_6]^{3+}$	-1838	-1838
$[Co(H_2O)_{18}]^{2+}$	-625	-625	$[Co(H_2O)_{18}]^{3+}$	-1299	-1295
$[Ni(H_2O)_6]^{2+}$	-809	-807	$[Ni(H_2O)_6]^{3+}$	-1782	-1779
$[Ni(H_2O)_{18}]^{2+}$	-623	-623	$[Ni(H_2O)_{18}]^{3+}$	-1285	-1286
$[Cu(H_2O)_6]^{2+}$	-810	-811	$[Cu(H_2O)_6]^{3+}$	-1805	-1798
$[Cu(H_2O)_{18}]^{2+}$	-637	-623	$[Cu(H_2O)_{18}]^{3+}$	-1287	-1289

5.3.3 Calculation of hydration enthalpy, $\Delta H^\circ_{\mathrm{hyd}}$

For calculation of hydration enthalpy according to eq 19 (in p. 27) we must add the experimental heat of vaporization of water ΔH_{vap}, 44.64 kJ/mol and a pressure work term ΔnRT to the calculated binding and solvation energies: ΔE_{b} and ΔE_{sol}. In our case Δn is equal to –6 or –18. Results of the calculations are shown in Table 5.

The differencies between the calculated and experimental hydration enthalpies for ions with charge 2+ are quite similar, no matter whether a 6-water or an 18-water complex is used. For the 6-water complexes the difference was from –208 up to –85 kJ/mol, for the 18-water complexes, from –142 up to –10 kJ/mol. For the ions with charges 3+ the difference was larger, from –223 up to –97 kJ/mol and from –55 up to 70 kJ/mol, respectively. The largest difference between the calculated hydration enthalpies and the experimental ones was observed for Co^{3+}, where the experimental and the calculated values differ as much as 285...474 kJ/mol, for the 6-water and 18-water clusters, respectively.

The transition metal ions in solution do not have the same charge as in the gas phase. Charge transfer follows the attachment of water molecules to a metal ion. The similarity of accuracies for the 6 and 18 water systems with charge 2+ may indicate that the first coordination sphere is sufficient for the modeling of the charge transfer in the system. For systems with charges 3+ six water molecules are not sufficient to accommodate the transferred charge and the larger water cluster models describe the charge transfer process in solution better.

The calculations affirm the essentiality of the second coordination shell in

Table 5: The calculated hydration enthalpies, in kJ/mol

Ion	$\Delta H^\circ_{\text{hyd}}$	Expt.[74]	Ion	$\Delta H^\circ_{\text{hyd}}$	Expt.[74]
$[Sc(H_2O)_6]^{2+}$	-1618	—	$[Sc(H_2O)_6]^{3+}$	-3791	—
$[Sc(H_2O)_{18}]^{2+}$	-1667	—	$[Sc(H_2O)_{18}]^{3+}$	-3923	—
$[Ti(H_2O)_6]^{2+}$	-1654	-1862	$[Ti(H_2O)_6]^{3+}$	-4026	-4154
$[Ti(H_2O)_{18}]^{2+}$	-1620	-1862	$[Ti(H_2O)_{18}]^{3+}$	-4173	-4154
$[V(H_2O)_6]^{2+}$	-1741	-1918	$[V(H_2O)_6]^{3+}$	-4155	-4375
$[V(H_2O)_{18}]^{2+}$	-1806	-1918	$[V(H_2O)_{18}]^{3+}$	-4333	-4375
$[Cr(H_2O)_6]^{2+}$	-1793	-1904	$[Cr(H_2O)_6]^{3+}$	-4337	-4560
$[Cr(H_2O)_{18}]^{2+}$	-1843	-1904	$[Cr(H_2O)_{18}]^{3+}$	-4505	-4560
$[Mn(H_2O)_6]^{2+}$	-1756	-1841	$[Mn(H_2O)_6]^{3+}$	-4396	-4544
$[Mn(H_2O)_{18}]^{2+}$	-1790	-1841	$[Mn(H_2O)_{18}]^{3+}$	-4574	-4544
$[Fe(H_2O)_6]^{2+}$	-1828	-1946	$[Fe(H_2O)_6]^{3+}$	-4333	-4430
$[Fe(H_2O)_{18}]^{2+}$	-1879	-1946	$[Fe(H_2O)_{18}]^{3+}$	-4500	-4430
$[Co(H_2O)_6]^{2+}$	-1878	-1996	$[Co(H_2O)_6]^{3+}$	-4936	-4651
$[Co(H_2O)_{18}]^{2+}$	-1933	-1996	$[Co(H_2O)_{18}]^{3+}$	-5125	-4651
$[Ni(H_2O)_6]^{2+}$	-1978	-2105	$[Ni(H_2O)_6]^{3+}$	-4678	—
$[Ni(H_2O)_{18}]^{2+}$	-2015	-2105	$[Ni(H_2O)_{18}]^{3+}$	-4883	—
$[Cu(H_2O)_6]^{2+}$	-2009	-2100	$[Cu(H_2O)_6]^{3+}$	-4866	—
$[Cu(H_2O)_{18}]^{2+}$	-2076	-2100	$[Cu(H_2O)_{18}]^{3+}$	-5062	—

the supermolecule approach. Only one coordination shell could be insufficient to model the solvation with a reasonable accuracy.

For Fe^{2+} and Fe^{3+} we have also calculated the hydration enthalpy with the third coordination shell. The values are summarized in Table 6.

The results confirm previous calculations. For Fe^{2+} the third solvation sphere is not essential, the difference between the experimental and the calculated values increases from -118 to -67 kJ/mol when the second sphere is added to the first one and when the third sphere was added then the difference is -145 kJ/mol.

For Fe^{3+} the third solvation sphere is more essential. The difference was -97 kJ/mol for the model involving only the first sphere. The calculated results overestimate the measured value 70 and 123 kJ/mol, for the second and third shells, respectively. As can be seen, the difference between the calculated and the

Table 6: Energetics of $[Fe(H_2O)_n]^{2+}$ and $[Fe(H_2O)_n]^{3+}$, in kJ/mol

Ion	ΔE_b	ΔE_{sol}	ΔH°_{hyd}	
			Calc.	Expt.[74]
$[Fe(H_2O)_6]^{2+}$	-1289	-792	-1828	-1946
$[Fe(H_2O)_{18}]^{2+}$	-2016	-622	-1879	-1946
$[Fe(H_2O)_{42}]^{2+}$	-2975	-597	-1801	-1946
$[Fe(H_2O)_6]^{3+}$	-2814	-1772	-4333	-4430
$[Fe(H_2O)_{18}]^{3+}$	-3978	-1280	-4500	-4430
$[Fe(H_2O)_{42}]^{3+}$	-5237	-1086	-4553	-4430

experimental results increases.

The hydration energy of the Sc^{2+}, Sc^{3+}, Ni^{3+} and Cu^{3+} ions do not appear to be determined experimentally. We have predicted[III] that the appropriate values should be follows: –1800 kJ/mol for Sc^{2+}, –3900 kJ/mol for Sc^{3+}, –4800 kJ/mol for Ni^{3+} and –4900 kJ/mol for Cu^{3+}. Later we found two different experimental values for the hydration enthalpy for Sc^{3+}: –3895[75] and –3960[1] kJ/mol. Our predicted value agrees with these experimental values.

5.4 Redox potentials

The gas phase and solution energetic data make it possible to compute the redox potentials of the M^{3+}/M^{2+} ions (M = Sc — Cu) in aqueous solution.

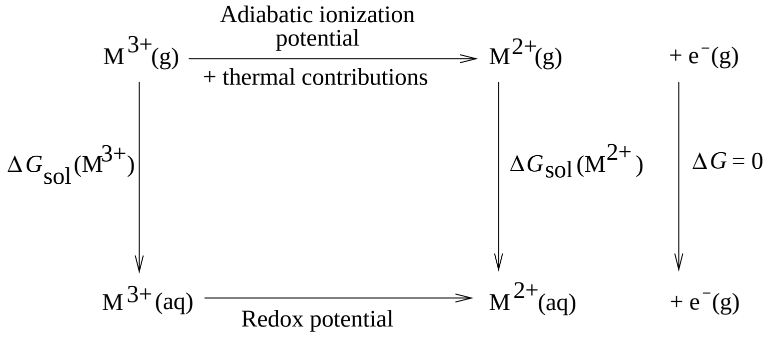
Adiabatic ionization potential
+ thermal contributions
M3+(g)
M2+(g)
+ e-(g)
ΔGsol(M3+)
ΔGsol(M2+)
ΔG = 0
M3+(aq)
M2+(aq)
+ e-(g)
Redox potential

Figure 11: The thermodynamic cycle defining redox potentials E_{redox}

The calculation of the redox potentials is based on the thermodynamic cycle shown in Figure 11,[13] which leads to the following equation:[13]

$$E^{\circ}_{redox} = \text{IP(g)} - \Delta\Delta E_{sol} + T\Delta S + \Delta E^{\circ}_{SHE} \tag{22}$$

where IP(g) is the computed gas phase ionization potential of the corresponding ion-water cluster, calculated as the difference of energies for the optimized geometries of the M^{3+} and M^{2+} cation complexes. Difference between the clusters zero-point vibrational energies was also added. The $\Delta\Delta E_{sol}$ represents the calculated solvation free energy of the ion-water clusters. It is the difference in continuum solvation energies and is found as a difference between the single-point COSMO calculation for the participating clusters.

We have used the experimental values of the entropy term, $T\Delta S$, and the standard hydrogen electrode potential, ΔE°_{SHE}. The entropy changes are found to play a crucial role in determining of the reduction potential. Quantum chemically calculations of ΔS failed: the difference between calculated and measured values was unreasonably large. In this work we have used values based on the temperature dependency data compiled by Bratsch,[76] where ΔS° is related to this:

$$\Delta S^{\circ}_{298} = nF\frac{dE^{\circ}}{dT_{298}} \tag{23}$$

Here F is the Faraday constant and n is number of electrons transfered (1 in the present study). The standard temperature of 298 K was used in eq 22.

In our earlier studies^{II} we used 4.43 eV[42] as the value for ΔE°_{SHE}. Recently this value has been recalculated and the enhanced value is 4.36 eV.[43] In this thesis we used the latest value. In Table 7 the gas phase and solution energetic data to compute the redox potentials are summarized.

Table 7: The calculated values, in V

System	Model	IP(g)	$\Delta\Delta E_{sol}$	$T\Delta S$
Sc^{3+}/Sc^{2+}	M^{3+}/M^{2+}	25.72	-15.89	0.48
	$[M(H_2O)_6]^{3+}/[M(H_2O)_6]^{2+}$	13.19	-9.99	0.48
	$[M(H_2O)_{18}]^{3+}/[M(H_2O)_{18}]^{2+}$	9.11	-6.77	0.48
Ti^{3+}/Ti^{2+}	M^{3+}/M^{2+}	28.65	-15.87	0.45
	$[M(H_2O)_6]^{3+}/[M(H_2O)_6]^{2+}$	14.18	-10.11	0.45
	$[M(H_2O)_{18}]^{3+}/[M(H_2O)_{18}]^{2+}$	10.05	-6.82	0.45
V^{3+}/V^{2+}	M^{3+}/M^{2+}	30.00	-15.70	0.45
	$[M(H_2O)_6]^{3+}/[M(H_2O)_6]^{2+}$	15.21	-10.23	0.45
	$[M(H_2O)_{18}]^{3+}/[M(H_2O)_{18}]^{2+}$	10.61	-6.80	0.45
Cr^{3+}/Cr^{2+}	M^{3+}/M^{2+}	31.10	-15.90	0.42
	$[M(H_2O)_6]^{3+}/[M(H_2O)_6]^{2+}$	15.10	-10.37	0.42
	$[M(H_2O)_{18}]^{3+}/[M(H_2O)_{18}]^{2+}$	10.42	-6.91	0.42
Mn^{3+}/Mn^{2+}	M^{3+}/M^{2+}	33.95	-15.91	0.54
	$[M(H_2O)_6]^{3+}/[M(H_2O)_6]^{2+}$	16.95	-10.35	0.54
	$[M(H_2O)_{18}]^{3+}/[M(H_2O)_{18}]^{2+}$	11.96	-6.85	0.54
Fe^{3+}/Fe^{2+}	M^{3+}/M^{2+}	31.97	-15.91	0.35
	$[M(H_2O)_6]^{3+}/[M(H_2O)_6]^{2+}$	16.16	-10.16	0.35
	$[M(H_2O)_{18}]^{3+}/[M(H_2O)_{18}]^{2+}$	11.63	-6.83	0.35
Co^{3+}/Co^{2+}	M^{3+}/M^{2+}	38.25	-15.91	0.37
	$[M(H_2O)_6]^{3+}/[M(H_2O)_6]^{2+}$	17.34	-10.78	0.37
	$[M(H_2O)_{18}]^{3+}/[M(H_2O)_{18}]^{2+}$	12.15	-6.99	0.37
Ni^{3+}/Ni^{2+}	M^{3+}/M^{2+}	37.58	-16.07	0.33
	$[M(H_2O)_6]^{3+}/[M(H_2O)_6]^{2+}$	18.21	-10.53	0.33
	$[M(H_2O)_{18}]^{3+}/[M(H_2O)_{18}]^{2+}$	12.94	-6.90	0.33
Cu^{3+}/Cu^{2+}	M^{3+}/M^{2+}	37.25	-15.91	0.45
	$[M(H_2O)_6]^{3+}/[M(H_2O)_6]^{2+}$	17.87	-10.24	0.45
	$[M(H_2O)_{18}]^{3+}/[M(H_2O)_{18}]^{2+}$	13.20	-6.91	0.45

5.4.1 Calculation of redox potentials

The calculated redox potentials are shown in Table 8. The gas-phase adiabatic ionization potential of ion is a very poor approximation to the aqueous redox potential. Differences from the experimental values are between 25 and 33 volts originated from the bare M^{3+} and M^{2+} ions. This can be expected since all the relaxation effects in the solvent are neglected in this approximation, leading to a gross over-estimation of the energy difference between the two oxidation states in the aqueous environment.

Surrounding of the central ion by the solvation shells is thus essential for obtaining a better accuracy. The first solvation shell (six water molecules in our model) decreases the differences from the experiment up to 11.17...11.88 volts. However it is significant that the differences are almost constant for all systems. Based on the present limited selection of ions, use of the adiabatic ionization potential of a hexa-aqua complex in the gas phase could be used as an estimate for the aqueous redox potential, if a correction of 11.53 volts (average for the ions in this study) is added.

Use of two explicitly-modeled solvation spheres (18 water molecules) reduces the difference between the calculated and the experimental values. Differences drop from 11.53 to an average of 6.85 volts. While the inclusion of the explicit second solvation sphere reduces the gap between the calculation and the experiment a little, it is clearly not sufficient alone to bring the results close to the experimental values.

The bare ion with a continuum solvation model (COSMO) does not improve the quality of the predictions significantly. Differences from the experiment are between 8 and 16 volt. Use of the default atomic radii, and neglection of the cavitation and dispersion terms are the main contributing factors to this failure.

Surrounding of the six-ligand model with a dielectric continuum brings the redox potentials into the experimental range. The values remain typically about 0.65...1.62 volts more positive. When the second coordination sphere is combined with a continuum model the resulting calculated redox potentials are approaching the experimental accuracy. Differences from the experiment are less than 0.5 volts in most cases, and better than 0.1 volts for chromium, iron, copper. The average absolute difference from the experiment across nine redox potentials is 0.28 V.

Use of three explicitly-modeled solvation spheres (42 water molecules) is computationally expensive. Due to this we have calculated the redox potential only for Fe^{3+}/Fe^{2+} using the third solvation sphere. As a large change in the geometry of the water cluster in the redox process could be improbable, we have used the similar minima for both ions (Figure 6, 7) and have found that the complex *B* (Figure 7 p. 22) has the lowest energy for the Fe^{3+} and Fe^{2+} central ions.

Table 8: The calculated and the experimental redox potentials, in V

	Ion			Ion				
		+ 6 H_2O	+ 18 H_2O		+ 6 H_2O	+ 18 H_2O		
System				+continuum model			Expt.	Ref.
Sc^{3+}/Sc^{2+}	21.84	9.31	5.23	5.95	-0.68	-1.54	-2.3	76
Ti^{3+}/Ti^{2+}	24.74	10.27	6.14	8.87	0.16	-0.68	-0.9	76
V^{3+}/V^{2+}	26.09	11.30	6.70	10.40	1.07	-0.10	-0.255	77
Cr^{3+}/Cr^{2+}	27.16	11.16	6.48	11.26	0.79	-0.43	-0.42	78
Mn^{3+}/Mn^{2+}	30.13	13.13	8.14	14.22	2.77	1.28	1.54	79
Fe^{3+}/Fe^{2+}	27.96	12.15	7.62	12.05	1.99	0.80	0.77	71
Co^{3+}/Co^{2+}	34.26	13.35	8.16	18.34	2.57	1.17	1.92	80, 81
Ni^{3+}/Ni^{2+}	33.55	14.18	8.91	17.47	3.65	2.01	2.3	76
Cu^{3+}/Cu^{2+}	33.34	13.96	9.29	17.43	3.73	2.39	2.4	76
AAD	28.22	11.53	6.85	12.33	1.22	0.28		

AAD - The average absolute difference from experimental values, d = $\frac{1}{n} \Sigma |x_{calc} - x_{expt}|$

Table 9: Difference between the calculated and the experimental Fe^{3+}/Fe^{2+} redox potentials, in V

	Fe^{3+}/ Fe^{2+}	$[Fe(H_2O)_6]^{3+}$/ $[Fe(H_2O)_6]^{2+}$	$[Fe(H_2O)_{18}]^{3+}$/ $[Fe(H_2O)_{18}]^{2+}$/	$[Fe(H_2O)_{42}]^{3+}$/ $[Fe(H_2O)_{42}]^{2+}$/
In gas phase	27.19	11.38	6.85	2.96
In continuum	11.28	1.22	0.03	-1.14

The gas phase calculations affirm the importance of the third solvation sphere in getting the better accuracy. The increase of the accuracy can be followed in Table 9. The difference between the calculated and the experimental redox potential is increased from 11.38 to 6.85 V in a gas phase or from 1.22 to 0.03 V in the continuum by adding to the first sphere the second solvation sphere. Adding of the third solvation sphere the correction is not so noticeable, from 6.85 to 2.96 V or from 0.03 to –1.14 V, respectively. At the same time the effect is not so determinative reckon with the time-consuming calculations.

The $[Fe(H_2O)_{42}]^{3+}/[Fe(H_2O)_{42}]^{2+}$ redox potential (calculated with the continuum model) is overestimated. One reason for that could be that our model. 24 water molecules is not sufficient to describe the third solvation sphere in the real solute. For the Fe^{3+} and Fe^{2+} the number of the surrounding molecules could be different. The ion with the higher charge, Fe^{3+}, is able to attract more solvent molecules than Fe^{2+}.[1]

5.4.2 Co^{3+}/Co^{2+} and Ni^{3+}/Ni^{2+}

For three redox pairs Sc^{3+}/Sc^{2+}, Co^{3+}/Co^{2+} and Ni^{3+}/Ni^{2+} the calculated potential values differ from experimental ones by –0.75...0.76 V (Table 8). We present some possible explanation for that in this section.

There are some uncertain points already in the experimental values: we have used the estimated values by Bratsch[76] for Sc^{3+}/Sc^{2+} and Ni^{3+}/Ni^{2+}. No primary source for those redox potentials could be established. For Co^{3+}/Co^{2+} there are several published values: 1.92 V,[80,81] 1.93 V,[82] 1.81 V,[83] 1.82-1.86 V,[84] 1.45 V.[85] We adopted 1.92 V as the reference value because there are two independent experimental measurements for the value.

The other reason could be some faults in our models. For example, the coordination number for Sc^{3+} in aqueous solution differ from six according to some Raman studies.[7] The Sc^{3+} ion has a small ionic radius and it could cause a favored coordination number of six and perhaps seven, and the presence of small amounts of octahedral $[Sc(H_2O)_6]^{3+}$ in equilibrium with $[Sc(H_2O)_7]^{3+}$ is possible.[1] Aqueous $[Co(H_2O)_6]^{2+}$ has been found in equilibrium with amounts of tetrahedral $[Co(H_2O)_4]^{2+}$.[9]

Checking the multiplicities of the ions could be another alternative. Sc^{3+}, Sc^{2+} are Ni^{2+} are the low spin, Co^{3+}, Co^{2+} and Ni^{3+} could be low- and high-spin. The low-spin nature of $[Co(H_2O)_6]^{3+}$ is reflected by the properties of the ion within the alum lattice.[1] High-spin is observed in the exited state.[86,87] The electron spectrum of $[Co(H_2O)_6]^{2+}$ characterizes the doublet (i.e low spin) state.[1] Richardson et al[88] have estimated the conversion of the low-spin Co^{3+} to the high-spin Co^{2+} from the experimental values of vibrational frequencies in hexa-ammine complexes. However, Kritayakornupong et al[37] used the high-spin state in Co^{3+} calculations. Schmiedekamp et al[89] have compared the high and the low spin configurations of Co^{2+} with biological ligands H_2O and NH_3 using the DFT methodology. The calculations predict that the high-spin state is more stable for Co^{2+}.

The studies for this thesis consist of the comparing of the relative energies, the reorganization energies and the structural changes of the Co^{3+}, Co^{2+} and Ni^{3+} clusters with two solvation spheres. The Co^{2+} high-spin system has lower energy. The difference between the low and the high spin complexes is 0.2 eV. Co^{3+} and Ni^{3+} are low-spin systems, the differences from the high-spin are 0.4 eV and 0.2 eV, respectively. The results are in good agreement with previous studies.[1,86–88]

Low-spin Co^{3+} and Ni^{3+} and high-spin Co^{2+} gave less accurate results in calculation of redox potentials. For Co^{3+}/Co^{2+} the difference between calculated and experimental results was –0.75 V and for Ni^{3+}/Ni^{2+} –0.29 V (Table 8 p. 36).

Use of the energy of a high-spin Co^{3+} and Ni^{3+} would lead to a value of redox potential that is much closer to the accepted experimental value (Table 10). The gap between experiment and calculation is –0.10 V and 0.01 V, respectively. Use of the low-spin Co^{3+} and Co^{2+} would lead to a significant discrepancy with the experimental value: –0.97 V.

Table 10: The calculated redox potentials $[M(H_2O)_{18}]^{3+}/[M(H_2O)_{18}]^{2+}$ (M = Co, Ni), in V

Systems	Orbitals	IP(g)	$\Delta\Delta E_{sol}$	Redox potentials	
				Calc.	Expt.
Co^{3+}/Co^{2+}	t_{2g}^6/ $t_{2g}^6 e_g^1$	11.95	-7.01	0.95	1.92[80,81]
	$t_{2g}^4 e_g^2/t_{2g}^5 e_g^2$	12.59	-6.78	1.82	1.92[80,81]
Ni^{3+}/Ni^{2+}	$t_{2g}^5 e_g^2/t_{2g}^6 e_g^2$	15.12	-8.78	2.31	2.3[76]

One way to express figuratively electron transfer is to represent the electronic structure of the ions. In a reduction process an electron is added to the lowest unoccupied molecular orbital (LUMO). Therefore, there should be a correlation between changes in the frontier orbitals and redox potentials due to changes in substitutents.

Electron transfer from Co^{3+} to Co^{2+} could occur in octahedral symmetry in three ways:

Co^{3+} (t_{2g}^6) + e^- → Co^{2+} ($t_{2g}^5e_g^2$)

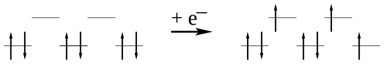

The singlet-quartet crossover. This is the case where both ions have lower energy (low-spin Co^{3+} and high-spin Co^{2+}) but as one pair of t_{2g} electrons must also split to form high-spin Co^{2+} from the low-spin Co^{3+}, this process should be unacceptable.

Co^{3+} (t_{2g}^6) + e^- → Co^{2+} ($t_{2g}^6e_g^1$)

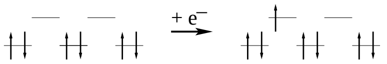

The singlet-doublet crossover. Adding an electron to the low-spin Co^{3+} the empty e_g (antibonding) orbital leads to he low-spin Co^{2+}.

Co^{3+} ($t_{2g}^4e_g^2$) + e^- → Co^{2+} ($t_{2g}^5e_g^2$)

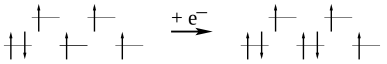

The quintet-quartet crossover. In the high-spin Co^{3+} one t_{2g} orbital is doubly occupied and the other t_{2g} and e_g orbitals are singly occupied. The electron is added to the partly occupied t_{2g} orbital. In this case the Co^{2+} is also high-spin.

For Ni^{3+}/Ni^{2+} there are two possibilities:

Ni^{3+} ($t_{2g}^6e_g^1$) + e^- → Ni^{2+} ($t_{2g}^6e_g^2$)

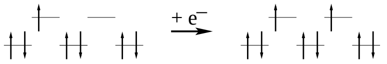

The quintet-triplet crossover arises from the low-spin Ni^{3+}. The electron is supplemented to the empty e_g orbital.

Ni^{3+} ($t_{2g}^5e_g^2$) + e^- → Ni^{2+} ($t_{2g}^6e_g^2$)

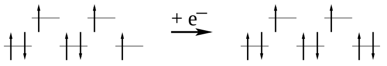

The quartet-triplet crossover originates from the high-spin Ni^{3+}. The electron is added to the t_{2g} orbital. Ni^{2+} has the same configuration in both cases.

We have used in comparison with the experimental and calculated redox potential the results of calculations of the model where the second coordination sphere is combined with a continuum. Observing the accuracy of calculated redox potentials (Table 11 p. 41) corresponded to previous, adding the electron to already singly occupied t_{2g} orbital gives more accurate results.

5.4.3 The reorganization energy

The reorganization energy is one of the major physical factors that controls the electron transfer reaction rates. For the electron transfer between molecules in which small changes in atomic charges are distributed over many atoms, the internal vibrational modes of the electron carriers are expected to make relatively minor contributions to the reorganization energy.[90]

The reorganization energy λ is the energy required to move all the precursor complex atoms, including the solvent molecules, from their equilibrium positions to the equilibrium positions of the successor complex without transferring the electron. λ consists of the inner sphere reorganization energies (λ_{is}) and the outer sphere solvent molecules reorganization energies (λ_{os}).[90]

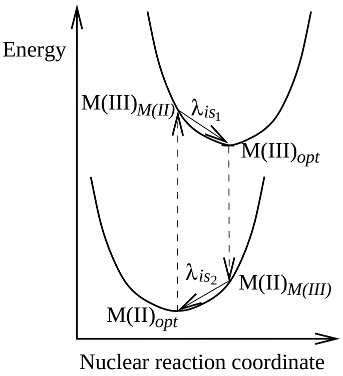

Figure 12: Calculation of reorganization energies

The inner sphere reorganization energy for the self-exchange reactions could be calculated from the ab initio total energy differences of four $[\mathrm{M(H_2O)_{18}}]^{m+}$ gas-phase clusters[90,91] (see Figure 12).

$$\lambda_{is} = \lambda_{is1} + \lambda_{is2} \tag{24}$$

where

$$\lambda_{is1} = E(\mathrm{M(III)}_{M(II)}) - E(\mathrm{M(III)}_{opt}) \tag{25}$$

$$\lambda_{is2} = E(\mathrm{M(II)}_{M(III)}) - E(\mathrm{M(II)}_{opt}) \tag{26}$$

Here M(III)$_{M(II)}$ represents a single point energy calculation of $[\mathrm{M(H_2O)_{18}}]^{3+}$ complex frozen in the optimized $[\mathrm{M(H_2O)_{18}}]^{2+}$ complex configuration and vice versa for M(II)$_{M(III)}$.

λ_{os} denotes the work of reorganizing solvent molecules surrounding the activated (donor and acceptor) complex and has been treated from the continuum theory[92] using:

$$\lambda_{os} = (\Delta q)^2 \left(\frac{1}{2r_{1\ M-O}} + \frac{1}{2r_{2\ M-O}} - \frac{1}{R} \right) \left(\frac{1}{D_{op}} - \frac{1}{\epsilon_s} \right) \tag{27}$$

where q is the charge transferred, r_1 and r_2 are the effective radii of the reactant molecules (M - O bond length), r_1 + r_2 = R, and D_{op} is the optical dielectric constant of the solvent (for water D_{op} = 1.78), ϵ_s is the static dielectric constant of the solvent (for water ϵ_s = 78.5). Unit of a bond length is in angstroms Å, the reorganization energy is in electron-volts, eV.

The values of λ for the $[M(H_2O)_{18}]^{m+}$ (M = Co, Ni, m = 2, 3) clusters in a gas phase are determined. The calculated inner and outer sphere reorganization energies and the structural changes of the clusters are summarized in Table 11. The difference between the calculated and the experimental redox potential is also given.

Table 11: Comparison of different multiplicities for Co^{3+}/Co^{2+} and Ni^{3+}/Ni^{2+}

System, orbitals	ΔE_{redox} V	Δr(M–O) Å	λ_{is} eV	λ_{os} eV	λ, calc. eV	λ, expt. eV
Co^{3+}/Co^{2+}						2.24[91]
$t_{2g}^6/t_{2g}^5e_g^2$	-0.75	0.16	3.24	0.97	4.21	
$t_{2g}^6/t_{2g}^6e_g^1$	-0.97	0.15	2.51	0.97	3.48	
$t_{2g}^4e_g^2/t_{2g}^5e_g^2$	-0.10	0.06	1.25	1.00	2.25	
Ni^{3+}/Ni^{2+}						
$t_{2g}^6e_g^1/t_{2g}^6e_g^2$	-0.29	0.10	1.98	0.99	2.97	
$t_{2g}^5e_g^2/t_{2g}^6e_g^2$	0.01	0.07	1.16	0.99	2.15	

The bond lengths in the transition metal complexes are unequal and depend on the d-configuration of the metal ion. The energies of the orbitals are not equivalent. The bonds of M^{3+} complex could increase and the bonds of M^{2+} complex could decrease until the participating orbitals have the same energy for electron transfer.[90]

Placing electron into the e_g levels leads to the extended M–O bonds, while adding the electron into the t_{2g} orbitals causes the smaller changes in the M–O bond length and decreases the reorganization (λ) energies.

In the electron transfer reactions the singlet-quartet and the singlet-doublet crossovers of Co^{3+}/Co^{2+} causes a substantial structural change compared with the quintet-quartet crossover. For Ni^{3+}/Ni^{2+} the quintet-triplet crossover is energetically more favored than the quartet-triplet crossover.

5.4.4 Calculation of redox potentials of MOH^{2+}, H^+/M^{2+}

To test the procedure of calculation of the redox potentials in the aqueous medium, the redox potentials of MOH^{2+}/M^{2+} in acidic solution are calculated. $CrOH^{2+}$, H^+/Cr^{2+} and $FeOH^{2+}$, H^+/Fe^{2+} are the two redox pairs in acidic solution where the reduced form is the metal ion (with a charge of 3+) with OH^- as a ligand and the oxidized form is a pure metal ion with a charge of 2+.

For the redox potential calculation a modification of equation 22 in p. 33 is used. Using the same steps as for M^{3+}/M^{2+}, the redox potentials for these systems are calculated, applying the previous data for Cr^{2+} and Fe^{2+}. More calculated energies must be taken into account for calculation of these redox potentials than in the previous M^{3+}/M^{2+} redox potentials calculations. There are two different ions in one side, MOH^{2+} and H^+ ions, and in the other side is the M^{2+} ion. The ions are surrounded by water molecules, thus the water cluster should be taken into account to model such systems quantum-chemically. From the point of view of computational electrochemistry the redox system is following:

$$[\mathrm{MOH(H_2O)}_{n-1}]^{2+}, [\mathrm{H(H_2O)}_n]^{+}/[\mathrm{M(H_2O)}_n]^{2+}, (\mathrm{H_2O})_n \tag{28}$$

The presence of the water cluster $(H_2O)_n$ (n = 6, 18) is a requirement for the equilibrium: for comparing of different systems the number of electrons and atoms must be equal.

The redox potential for MOH^{2+}, H^+/M^{2+} can be calculated using eq 28 as a model:

$$\begin{aligned} E^\circ_{redox} \;=\; & E[\mathrm{MOH(H_2O)}_{n-1}\mathrm{(ZPE)}]^{2+} + E[\mathrm{H(H_2O)}_n\mathrm{(ZPE)}]^{+} \\ & -E[\mathrm{(H_2O)}_n\mathrm{(ZPE)}] - E[\mathrm{M(H_2O)}_n\mathrm{(ZPE)}]^{2+} - E[\mathrm{(H_2O)}_n\mathrm{(g)}] \\ & +E[\mathrm{MOH(H_2O)}_{n-1}\mathrm{(COSMO)}]^{2+} + E[\mathrm{H(H_2O)}_n\mathrm{(COSMO)}]^{+} \\ & -E[\mathrm{M(H_2O)}_n\mathrm{(COSMO)}]^{2+} + T\Delta S + \Delta E^\circ_{SHE} \end{aligned} \tag{29}$$

All needed energies are taken into account and are canceled where it was possible.

Table 12: The calculated and the experimental MOH^{2+}, H^+/M^{2+} redox potentials, in V

	Ion		
	+ first solv. sphere	+ second solv. sphere	Expt.[76]
$CrOH^{2+}$, H^+/Cr^{2+}	-1.16	-2.29	-0.19
$FeOH^{2+}$, H^+/Fe^{2+}	-0.26	-1.33	0.9

The calculated redox potentials are shown in Table 12. The calculated and the experimental data do not have a good agreement. The discrepancy between the experimental and the calculated results increases for both systems when he second solvation sphere is added. The difference between the experimental and the calculated redox potentials increases from -0.97 upto -2.10 V for $CrOH^{2+}$, H^{+}/Cr^{2+} and from -1.16 upto -2.23 V for $FeOH^{2+}$, H^{+}/Fe^{2+}.

In these calculations the importance of the second solvation sphere was not confirmed. Great importance of the water cluster must be taken into account. The modeled $[MOH(H_2O)_{17}]^{2+}$ cluster could not describe well the real situation in the solution.

It seems that the larger cluster gives a better approximation to the real solution but for that kind of systems using the ion and the first solvation sphere and the continuum model gives more accurate results than using two spheres and the continuum model. The "model" does not work for that kind of systems, unfortunately. The reason of this could be the circumstance that in $[MOH(H_2O)_{n-1}]^{2+}$ (M = Cr, Fe; n = 6, 18) complex the central ion M^{3+} has different ligands, there is one OH^{-} ligand and five H_2O ligands.

6 Conclusions

Solvation of the of the first row transition metals (Sc, Ti, V, Cr, Mn, Fe, Co, Ni, Cu) di- and trivalent ions was modeled in this thesis. As a result of DFT calculations the following conclusions have been made:

A. Application of two explicitly-modeled solvation spheres (18 water molecules) reduces the difference between the calculated and the experimental hydration enthalpies. The same is valid for the redox potential values. The second solvation shell is essential in the supermolecule approach. The use of the third solvation sphere was not so effective as use of the second shell;

B. Situations exist, where the continuum solvation model can not be employed for an open-shell system. Solvation energies were compared, for cases where the energies were calculated directly and when the open-shell central ions were exchanged with similarly-charged closed-shell species. The difference was -3...7 kJ/mol in most cases. The central ion substitution can be recommended in cases where the open-shell continuum calculations can not be carried out directly;

C. Hydration enthalpies for the di- and trivalent cations of the first row transition metals, Sc — Cu, were calculated and the results were compared with the experimental data. For M^{2+} the difference between the calculated and the experimental hydration entalpies for the 18-water complexes was from –142 upto –10 kJ/mol, for M^{3+} the difference was from –55 upto 70 kJ/mol. The values of hydration enthalpies for Sc^{2+}, Ni^{3+} and Cu^{3+} ion were predicted: Sc^{2+} –1800 kJ/mol, Ni^{3+} –4800 kJ/mol and Cu^{3+} –4900 kJ/mol;

D. The aqueous redox potentials of the transition metal ion pairs, M^{3+}/M^{2+} (M = Sc — Cu) were calculated. The calculated redox potentials are approaching the experimental accuracy. Differences from the experiment are less than 0.5 V in most cases, and better than 0.1 V for chromium, iron, copper;

E. The aqueous redox potentials for the following redox systems were calculated, MOH^{2+}, H^{+}/M^{2+} (M = Cr, Fe). The calculated and the experimental data were not in a good agreement. The difference was –1.16...–0.97 V using the ion and the first solvation sphere and –2.23...–2.10 V after adding the second sphere.

Abstract

The goal of this work was to investigate the possibilities of quantum chemical method to model solvation. In this thesis the first row transition metals (Sc, Ti, V, Cr, Mn, Fe, Co, Ni, Cu) di- and trivalent ions have been studied. For a hexa-aqua complex the second solvation sphere can model 12 water molecules and the third one 24 water molecules, bound via a hydrogen bonded to each of the hydrogen atoms of the previous solvation sphere.

The purpose of this work was to study the importance of the second solvation sphere. Development of the computational facilities and the software has made it possible to model two and three coordination spheres around the metal ions with high-level (eg TZVPP) basis sets. Unfortunately, calculations with three solvation shells were time consuming and a systematic research has not been done.

The accuracy of the methodology was assessed by the comparison with the experimental values. Firstly hydration enthalpies for M^{2+} and M^{3+}, (M = Sc — Cu) were calculated. The results affirmed the importance of the second solvation shell. The differences between the calculated and the experimental values for $[M(H_2O)_{18}]^{2+}$ complexes were –142...–10 kJ/mol, for $[M(H_2O)_{18}]^{3+}$ complexes —55...70 kJ/mol.

Secondly redox potentials for M^{3+}/M^{2+} (M = Sc — Cu) were calculated. The use of two explicitly modeled solvation spheres also reduces the differences between he calculated and the experimental values. The average absolute difference from the experimental values is 0.28 V, with three out of nine potentials (those of Cr, Fe, Cu) reproduced with better than 0.1 V accuracy. In this thesis is studied less accurately calculated redox pairs (Co and Ni) slightly.

The aqueous redox potentials for the redox systems MOH^{2+}, H^+/M^{2+} (M = Cr, Fe) were calculated. The differences between he calculated and the experimental values was –2.23...–2.10 V.

Kokkuvõte

Käesolevas töös uuriti üheksa üleminekumetalli (Sc, Ti, V, Cr, Mn, Fe, Co, Ni, Cu) solvateeritud iooni kvantkeemilist modelleerimist. Ioonide laenguteks olid vastavalt kas 2+ või 3+. Neid katioone ümbritseb vesilahuses kuus vee molekuli, mis moodustavad esimese solvatatsioonisfääri. Kui vesiniksideme abil siduda omakorda üks vee molekul iga esimeses solvatatsioonisfääris oleva vee molekuli vesiniku aatomiga, saame 12 vee molekulist koosneva teise solvatatsioonisfääri. Sarnaselt toimides saab ka modelleerida kolmandat solvatatsioonisfääri, mis koosneb 24 vee molekulist.

Antud töö eesmärgiks oli uurida, kui oluline on lahuse modelleerimisel teine solvatatsioonisfäär, samas annavad olemasolevad arvutuslikud võimsused võimaluse uurida kolmanda sfääri mõju arvutustäpsustele. Kahjuks olid aga viimased arvutused väga aeganõudvad, seetõttu süstemaatilist võrdlust läbi ei viidud.

Hindamaks kasutatud kvantkeemiliste mudelite täpsust, arvutati hüdratatsioonientalpiad M^{2+} ja M^{3+}, (M = Sc — Cu) katioonidele ning leiti, et teise sfääri kvantkeemiline kirjeldamine annab eksperimendile lähedasema tulemuse: $[M(H_2O)_{18}]^{2+}$ komplekside korral oli vahe –142...–10 kJ/mol, $[M(H_2O)_{18}]^{3+}$ puhul aga –55...70 kJ/mol. Kuna meie käsutuses polnud hüdratsioonientalpiaid Sc^{2+}, Ni^{3+} ja Cu^{3+} ioonide jaoks, siis tuginedes oma töö tulemustele, pakume nende vääruseks vastavalt: Sc^{2+} –1800 kJ/mol, Ni^{3+} –4800 kJ/mol ja Cu^{3+} –4900 kJ/mol.

Samuti arvutati redokspotentsiaali väärtused M^{3+}/M^{2+} (M = Sc — Cu) redokspaaridele ning võrreldi saadud tulemusi eksperimentaalsete väärtustega. Ka siin leidis kinnitust teise solvatatsioonisfääri olulisus suurema arvutustäpsuse saavutamisel. Keskmine erinevus oli 0.28 V, kõige väiksem oli erinevus (alla 0.1 V) kroomi, raua ja vase ioonide vaheliste redokspotentsiaalide arvutamisel. Suurema erinevuse andsid koobalti ja nikli redokspotentsiaalide arvutused ja seetõttu analüüsiti neid redokspaare lähemalt.

Arvutati ka redokspotentsiaale süsteemidele MOH^{2+}, H^+/M^{2+}, M = Cr, Fe, kuid kahjuks erinevus eksperimendiga oli suur, –2.23...–2.10 V.

References

1 Richens, D. T. *The Chemistry of Aqua Ions*. John Wiley & Sons Ltd, 1997.

2 Rudolph, W.; Brooker, M. H.; Pye, C. C. *J. Phys. Chem*, **1995**, *99*, 3793–3797.

3 Pye, C. C.; Rudolph, W. W. *J. Phys. Chem. A*, **1998**, *102*, 993–994.

4 Rudolph, W. W.; Pye, C. C. *J. Phys. Chem. B*, **1998**, *102*, 3564–3573.

5 Rudolph, W. W.; Pye, C. C. *Phys. Chem. Chem. Phys*, **1999**, pp 4583–4593.

6 Rudolph, W. W.; Mason, R.; Pye, C. C. *Phys. Chem. Chem. Phys*, **2000**, pp 5030–5040.

7 Rudolph, W. W.; Pye, C. C. *J. Phys. Chem.*, **2000**, *104*, 1627–1639.

8 Greenwood, N. N.; Earnshaw, A. *Chemistry of the Elements*. Reed Educational and Professional Publishing Ltd, second edition, 1997.

9 Inada, Y.; Hayashi, H.; Sugimoto, K.; Funahashi, S. *J. Phys. Chem. A*, **1999**, *103*, 1401–1406.

10 Tachikawa, H.; Ichikawa, T.; Yoshida, H. *J. Am. Chem. Soc.*, **1990**, *112*, 982–987.

11 Åkersson, R.; Pettersson, L. G. M.; Sandström, M.; Wahlgren, U. *J. Am. Chem. Soc.*, **1994**, *116*, 8691–8704.

12 Rotzinger, F. P. *J. Am. Chem. Soc.*, **1996**, *118*, 6760–6766.

13 Li, J.; Fisher, C. L.; Chen, J. L.; Bashford, D.; Noodleman, L. *Inorg. Chem.*, **1996**, *35*, 4694–4702.

14 Hartmann, M.; Clark, T.; van Eldik, R. *J. Phys. Chem. A*, **1999**, *103*, 9899–9905.

15 Kallies, B.; Meier, R. *Inorg. Chem.*, **2001**, *40*, 3101–3112.

16 Atkins, P. W. *Physical Chemistry*. Oxford University Press, sixth edition edition, 1998.

17 Lister, S. G.; Reynolds, C. A.; Richards, W. G. *Int. J. Quant. Chem.*, **1992**, *41*, 293–310.

18 Dubois, V.; Archirel, P.; Boutin, A. *J. Phys. Chem. B*, **2001**, *105*, 9363–9369.

19 Cora, I. S. F.; Alfredsson, M.; Catlow, C. R. A. *J. Phys. Chem. B*, **2003**, *107*, 3012–3018.

20 Baik, M.-H.; Crystal, J. B.; Friesner, R. A. *Inorg. Chem*, **2002**, *41*, 5926–5927.

21 Baik, M.-H.; Friesner, R. A. *J. Phys. Chem. A*, **2002**, *106*, 7407–7412.

22 Baik, M.-H.; Scauer, C. K.; Ziegler, T. *J. Am. Chem. Soc.*, **2002**, *124*, 11167–11181.

23 Fu, Y.; Liu, L.; Yu, H.-Z.; Wang, Y.-M.; Guo, Q.-X. *J. Am. Chem. Soc.*, **2005**, *127*, 7227–7234.

24 Dutton, A. S.; Fukuto, J. M.; Houk, K. N. *Inorg. Chem*, **2005**, *44*, 4024–4028.

25 Bachmann, J.; Nocera, D. G. *J. Am. Chem. Soc.*, **2005**, *127*, 4730–4743.

26 Kobayashi, H.; Miura, T.; Shimodiara, Y.; A.Kudo. *Chem. Lett.*, **2004**, *33*(9), 1176–1177.

27 Blumberger, J.; Bernasconi, L.; Tavernelli, I.; Vuilleumier, R.; Sprik, M. *J. Am. Chem. Soc.*, **2004**, *126*, 3928–3938.

28 Ichieda, N.; Kasuno, M.; Banu, K.; Kihara, S.; Nakamatsu, H. *J. Phys. Chem. A*, **2003**, *107*, 7597–7603.

29 Asthagiri, D.; Pratt, L. R.; Paulaitis, M. E.; Rempe, S. B. *J. Am. Chem. Soc.*, **2004**, *126*, 1285 – 1289.

30 Pye, C. C.; Rudolph, W. W. *J. Phys. Chem. A*, **1998**, *102*, 9933–9943.

31 Rudolph, W. W.; Pye, C. C. *J. Phys. Chem. B*, **1998**, *102*, 3564–3573.

32 Rudolph, W. W.; Pye, C. C. *Phys. Chem. Chem. Phys.*, **1999**, pp 4583–4593.

33 Rudolph, W. W.; Pye, C. C. *J. Phys. Chem. A*, **2000**, *104*, 1627–1639.

34 Rudolph, W. W.; Mason, R.; Pye, C. C. *Phys. Chem. Chem. Phys.*, **2000**, pp 5030–5040.

35 Pye, C. C. *Int. J. Quant. Chem.*, **2000**, *76*, 62–76.

36 Mejias, J. A.; Lago, S. *J. Chem. Phys.*, **2000**, *113*, 7306–7316.

37 Kritayakornupong, C.; Plankensteiner, K.; Rode, B. M. *J. Phys. Chem. A*, **2003**, *107*, 10330–10334.

38 Remsungnen, T.; Rode, B. M. *J. Phys. Chem. A*, **2003**, *107*, 2324–2328.

39 Remsungnen, T.; Rode, B. M. *Chem. Phys. Lett.*, **2004**, *385*, 491–497.

40 Kritayakornupong, C.; Plankensteiner, K.; Rode, B. M. *J. Comput. Chem.*, **2004**, *25*, 1576–1583.

41 Martinez, J. M.; Pappalardo, R. R.; Marcos, E. S. *J. Phys. Chem. A*, **1997**, *101*, 4444–4448.

42 Reiss, H.; Heller, A. *J. Phys. Chem*, **1985**, *89*, 4207–4213.

43 Lewis, A.; Bumpus, J. A.; Truhlar, D. G.; Cramer, C. J. *J. Chem. Educ.*, **2004**, *81*, 596–603.

44 Young, D. C. *Computational chemistry: a practical guide for applying tehniques to real world problems*. John Wiley & Sons, Inc, 2001.

45 Lewars, E. *Computational Chemistry: Introduction to the Theory and Applications of Molecular and Quantum Mechanics*. Kluwer Academic Publishers, 2003.

46 Kohn, W.; Sham, L. J. *Phys. Rev.*, **1965**, *140*, A1133–A1138.

47 Becke, A. D. *Phys. Rev. A*, **1988**, *38*(3098-3100).

48 Lee, C.; Yang, W.; Parr, R. G. *Phys. Rev. B*, **1988**, *37*, 785–789.

49 Perdew, J. P. *Phys. Rev. B*, **1986**, *33*, 8822–8824.

50 Becke, A. D. *J. Chem. Phys.*, **1993**, *98*, 5648–5652.

51 Erras-Henauer, H.; Clark, T.; van Eldik, R. *Coord. Chem. Rev.*, **2003**, *238-239*, 233–253.

52 Miertuŝ, S.; Scrocco, E.; Tomasi, J. *Chem. Phys.*, **1981**, *55*, 117–129.

53 Klamt, A.; Schüürmann, G. *J. Chem. Soc. Perkin Trans. 2.*, **1993**, pp 799–805.

54 Moskaleva, L. V.; Krüger, S.; Spörl, A.; Rösch, N. *Inorg. Chem.*, **2004**, *43*, 4080–4090.

55 Tauber, M. J.; Mathies, R. A. *J. Am. Chem. Soc.*, **2003**, *125*, 1394–1402.

56 Pye, C. C.; Rudolph, W.; Poirier, R. A. *J. Phys. Chem.*, **1996**, *100*, 601–605.

57 Zumdahl, S. S. *Chemical Principles*. Houghton Mifflin Company, third edition edition, 1998.

58 Schäfer, A.; Huber, C.; Ahlrichs, R. *J. Chem. Phys.*, **1994**, *100*, 5829–5835.

59 Uudsemaa, M. Quantum-chemical modeling of solvated titanium and vanadium ions. Master's thesis, Tallinn University of Technology, 2002.

60 Eichkorn, K.; Weigend, F.; Treutler, O.; Ahlrichs, R. *Theoret. Chim. Acta (Berl.)*, **1997**, *97*, 119–124.

61 Eichkorn, K.; Treutler, O.; Öhm, H.; Häser, M.; Ahlrichs, R. *Chem. Phys. Lett.*, **1995**, *240*, 283–289.

62 Eichkorn, K.; Weigend, F.; Treutler, O.; Ahlrichs, R. *Theor. Chem. Acc.*, **1997**, *97*, 119–124.

63 Weigend, F. *PCCP*, **2002**, *4*, 4285 – 4291.

64 Vahtras, O.; Almlöf, J.; Feyereisen, M. W. *Chem. Phys. Lett.*, **1993**, *213*, 514–517.

65 Schäfer, A.; Horn, H.; Ahlrichs, R. *J. Chem. Phys.*, **1992**, *97*, 2571–2577.

66 Cramer, C. J.; Truhlar, D. G. *Chem. Rev.*, **1999**, *99*, 2161–2200.

67 Klamt, A. *J. Phys. Chem.*, **1995**, *99*, 2224–2235.

68 Senn, H. M.; Margl, P. M.; Schmid, R.; Ziegler, T.; Blöchl, P. E. *J.Chem. Phys.*, **2003**, *118*, 1089–1100.

69 Markham, G. D.; Glusker, J. P.; Bock, C. W. *J. Phys. Chem. B.*, **2002**, *106*, 5118–5134.

70 Benmelouka, M.; Messaoudi, S.; Furet, E.; Gautier, R.; Fur, E. L.; Pivan, J.-Y. *J. Phys. Chem. A.*, **2003**, *107*, 4122–4129.

71 Schumb, W. C.; Sherrill, M. S.; Sweetser, S. B. *J. Am. Chem. Soc.*, **1937**, *59*, 2360–2365.

72 Whittemore, D. O.; Langmuir, D. *J. Chem. Eng. Data*, **1972**, *17*, 288–290.

73 Magini, M.; Licheri, G.; Paschina, G.; Piccaluga, G.; Pinna, G. *X-ray Diffraction of Ions in Aqueous Solutions: Hydration and Complex Formation*. CRC Press: Boca Ration, FL, 1988.

74 Smith, D. W. *J. Chem. Educ.*, **1977**, *54*(9), 540–542.

75 Smith, D. W. *J. Chem. Educ.*, **1977**, *54*, 540.

76 Bratsch, S. G. *J. Phys. Chem. Ref. Data*, **1989**, *18*, 1–21.

77 Jones, G.; Colvin, J. H. *J. Am. Chem. Soc.*, **1944**, *66*, 1563–1571.

78 von Grube, G.; Schlecht, L. *Z. Electrochem*, **1926**, *32*, 178–186.

79 Ciavatta, L.; Grimaldi, M. *J. Inorg. Nucl. Chem.*, **1969**, *31*, 3071–3082.

80 Diebler, H.; Sutin, N. *J. Phys. Chem*, **1964**, *68*, 174–180.

81 Huchital, D. H.; Sutin, N.; Warnqvist, B. *Inorg. Chem.*, **1967**, *6*, 838–840.

82 Johnson, D. A.; Sharpe, A. G. *J. Chem. Soc.*, **1964**, pp 3490–3492.

83 Rock, P. A. *Inorg. Chem.*, **1968**, *7*, 837–840.

84 Warnqvist, B. *Inorg. Chem.*, **1970**, *9*, 682–684.

85 Rotinjan, A. L.; Borisowa, L. M.; Boldin, R. W. *Electrochim. Acta*, **1974**, *19*, 43–46.

86 Winkler, J. R.; Rice, S. F.; Gray, H. B. *Comments Inorg. Chem.*, **1981**, *1*, 47–51.

87 Korotin, M. A.; Ezhov, S. Y.; Anisimov, V. I.; Khomskii, D. I.; Sawatzki, G. A. *Phys. Rev. B*, **1996**, *54*(8), 5309–5316.

88 Richardson, D. E.; Sharpe, P. *Inorg. Chem.*, **1991**, *30*, 1412–1414.

89 Schmiedekamp, A. M.; Ryan, M. D.; Deeth, R. J. *Inorg. Chem*, **2002**, *41*, 5733–5743.

90 Huheey, J. E.; Keiter, E. A.; Keiter, R. L. *Inorganic Chemistry: Principles of Structure and Reactivity*. HarperCollins College Publishers, fourth edition, 1993.

91 Rosso, K. M.; Rustad, J. R. *J. Phys. Chem. A.*, **2000**, *104*, 6718–6725.

92 Marcus, R. A. *J. Chem. Phys.*, **1956**, *24*,

966–978

.

Reproduced with permission from Chemical Physics Letters, Vol. 342,
pp. 667-672. Copyright 2001 Elsevier Science B. V.

ARTICLE I

M. Uudsemaa and T. Tamm, Calculations of hydrated titanium ion complexes: structure and influence of the first two coordination spheres. Chemical Physics Letters, **2001**, *342*, 667-672.

a

a

a

a

a

a

Reproduced with permission from Journal of Physical Chemistry A, Vol. 107, pp. 9997-10003. Copyright 2003 American Chemical Society.

ARTICLE II

M. Uudsemaa and T. Tamm, Density-functional theory calculations of aqueous redox potentials of fourth-period transition metals. Journal of Physical Chemistry A, **2003**, *107*, 9997-10003.

a

a

a

a

a

a

a

Reproduced with permission from Chemical Physics Letters, Vol. 400, pp. 54-58.
Copyright 2004 Elsevier Science B. V.

ARTICLE III

M. Uudsemaa and T. Tamm, Calculation of hydration enthalpies of aqueous transition metal cations using two coordination spheres and central ion substitution. Chemical Physics Letters, **2004**, *400*, 54-58.

a

a

a

a

a

Curriculum Vitae

Personal data

First and surname	Merle Uudsemaa
Date and place of birth	22.04.1971, Tallinn
Citizenship	Estonian
Children	Son, born 18.09.1995

Contact

Address	Department of Chemistry, Tallinn University of Technology, Akadeemia tee 15, Tallinn
Phone	+372 6202811
e-mail	merle@yki.ttu.ee

Education

2002	Tallinn Technical University, Master of Natural Sciences
1994	Tallinn Technical University, Engineer, Food Technology
1989	Tallinn Secondary School No 9

Professional	**Employment**
1999 - ...	Tallinn University of Technology, Department of Chemistry, research scientist
1994 - 2000	Tallinn City Court

Scientific work

Main topics of research: Quantum-chemical modeling of solvated metal ions

Elulookirjeldus

Isikuandmed

Ees- ja perekonnanimi	Merle Uudsemaa
Sünniaeg ja-koht	22.04.1971, Tallinn
Kodakondsus	Eesti
Perekonnaseis	Abielus
Lapsed	Poeg, sündinud 18.09.1995

Kontaktandmed

Aadress	Keemiainstituut, Tallinna Tehnikaülikool Akadeemia tee 15, Tallinn
Telefon	+372 6202811
E-posti aadress	merle@yki.ttu.ee

Hariduskäik

2002	Tallinna Tehnikaülikool, Loodusteaduste magister
1994	Tallinna Tehnikaülikool, Toiduainekeemia ja -tehnoloogia eriala, insener
1989	Tallinna 9. Keskkool

Teenistuskäik

1999 - ...	Tallinna Tehnikaülikool, teadur
1994 - 2000	Tallinna Linnakohtu täitevosakond, kohtutäitur

Kaitstud lõputööd

Magistritöö teema – “Titaani ja vanaadiumi solvateeritud ioonide kvantkeemiline modelleerimine”, juhendaja prof. T. Tamm
Diplomitöö teema – “Naturaalsete punaste toiduvärvide saamine ja omadused”, juhendaja A. Hamburg

Teadustöö põhisuunad

Metallikomplekside kvantkeemilised arvutused